Interactive Comment on: "Modelling debris transport within glaciers by advection in a full-Stokes ice flow model" by A. Wirbel et al.

Anna Wirbel[1], Alexander Helmut Jarosch[2], and Lindsey Nicholson[1]

[1]Institute of Atmospheric and Cryospheric Sciences, University of Innsbruck, Innsbruck, Austria
[2]Institute of Earth Sciences, University of Iceland, Reykjavík, Iceland

We thank the editor and the referees for their helpful comments on our manuscript. This document contains a detailed point by point response to the referees' comments and a version of the revised manuscript where changes in respect to the first version are highlighted using *latexdiff*. Additionally, we included a new figure (now Fig. A4) and an animation in the supplementary material showing the velocity fields used in the 2D and 3D benchmark tests. The other figures have also been edited according to the referee's comments and to improve print quality.

1 Response to Garry Clarke

We would like to thank Garry Clarke for his thorough and valuable review and for providing helpful comments on our manuscript.

1.1 Specific Comments

Comment: *For me the main source of confusion was whether a dimensional or dimensionless treatment was being followed. I got the impression that in fact both points of view were being taken but that the dividing lines were unclear. For example, the debris diffusivity D has dimensions $\mathrm{m}^{-2}\ \mathrm{s}^{1}$ (as it appears in Equation 5a) but on Page 9, Line 14 $D = 10^{-6}$ suggests it has become dimensionless for the LeVeque test. Contributing to this confusion is the fact that time steps of $0.01\,\pi$ and $0.1\,\pi$ (dimensionless?) and mesh sizes of $L_{csize} = 0.15\ \mathrm{m}$ are discussed on the same page. Please clarify here and elsewhere.*

Response: Thanks for this comment, we were not completely clear about this point. We follow a dimensional treatment throughout this study. In the case of the "rotating three body problem" (de Frutos et al., 2014) (Sect. 4.1), we enlarge the computational domain from $\Omega = (0,1) \times (0,1)$ to $\Omega = (0,100) \times (0,100)$ meters in order to allow direct evaluation of the performance of chosen mesh refinement thresholds, which have units, that we apply in the glacier cases. In this manner, the size of concentration features in the test case becomes comparable to that of the concentration features in the glacier cases. This allows us to evaluate the suitability of chosen mesh refinement thresholds (c_{vol} and L_{csize}) that we also apply in the presented glaciological applications. To facilitate the understanding of dimensions used, as well as to highlight the actual equation we solve in our model, we have added Eq. 1 (Equation 6a in the revised manuscript) to the manuscript. Assuming an

incompressible fluid and a constant diffusivity (D), Eq. 5a becomes:

$$\frac{\partial c}{\partial t} = D\nabla^2 c - \boldsymbol{u} \cdot \nabla c. \tag{1}$$

The assumptions used here have been stated in the manuscript. From Eq. 1 above it becomes apparent that D has the dimensions of $\mathrm{m}^2\ \mathrm{s}^{-1}$ when c is assumed to be dimensionless, as it is in our study. Timesteps as multiples of π in the advection tests stem from the angular velocity chosen in the de Frutos tests (de Frutos et al., 2014), where a whole rotation takes 2π seconds. We have clarified the dimensional approach we take in the manuscript by adding information on the dimensions of parameters at the following locations in the manuscript:

- $D = 10^{-6}\ \mathrm{m}^2\ \mathrm{s}^{-1}$, Page 9 Line 14; (Page 9 Line 14 in revised manuscript)
- $\Omega = (0,100) \times (0,100)$ meters, Page 9 Line 15; (Page 9 Line 15 in revised manuscript)
- $0.01\,\pi$ s; $0.1\,\pi$ s, Page 9 Line 19; (Page 9 Line 19 in revised manuscript)
- $2\,\pi$ s (T), Page 9 Line 20; (Page 9 Line 20 in revised manuscript)
- T, at $t = 1.5$ s, Page 9 Line 26; (Page 9 Line 28 in revised manuscript)
- $2\,\pi$ s (T), Page 9 Line 30; (Page 9 Line 31 in revised manuscript)
- $\Omega = (0,32) \times (0,32) \times (0,40)$ meters, Page 9 Line 31; (Page 9 Line 32 in revised manuscript)
- $0.04\,\pi$ s, Page 9 Line 32; (Page 9 Line 33 in revised manuscript)
- $0.1\,\pi$ s, Page 12 Line 14; (Page 13 Line 8 in revised manuscript)
- $2\,\pi$ s, Page 12 Line 15; (Page 13 Line 9 in revised manuscript)
- $0.01\,\pi$ s; $0.1\,\pi$ s, Page 13 Line 4 and captions of Figs. 6-7; (Page 13 Line 18 in revised manuscript)
- $dt = 0.1$ s, $dt = 0.01$ s, $dt = 0.001$ s, $dt = 0.0005$ s, $t = 0.5$ s, $y = 0.6$ m, $x = 0.75$ m, $y = 0.85$ m, $x = 1.0$ m, Page 2 Lines 1-4, Lines 10-11, Line 13 and captions of Figs. A2-A5 in the supplementary material (Page 2 Lines 1-4, Line 11, Lines 15-16 and captions of Figs. A2-A3 and A5-A6 in revised supplementary material)

1.2 Technical Corrections

We thank Garry Clarke for the careful reading of the manuscript and adapted the text to meet the suggested Technical Corrections.

Comment: *Figure 1 The caption should read "Kennicott Glacier" (spelling)*
Response: Corrected.

Comment: *P03, L29 "Eulerian" (not Eularian)*

Response: Corrected.

Comment: *P10, L04 917* $\mathrm{kg\ m^{-3}}$

Response: Inserted space.

Comment: *P10, L30* $x = 1800$ *m and* $x = 1900$ *m*

Response: Inserted units.

Comment: *P20, L19 Bozhinskiy et al. (1986): Check caps style*

Response: We checked the reference Bozhinskiy et al. (1986) and adapted the capitalization of the title according to the reference style used in The Cryosphere.

Comment: *P20, L28 Glen (1955): Check caps style*

Response: We checked the reference Glen (1955) and adapted the capitalization of the title according to the reference style used in The Cryosphere.

Comment: *P21, L07 John and Novo (2011): Check caps style*

Response: We checked the reference John and Novo (2011) and adapted the capitalization of the title according to the reference style used in The Cryosphere.

Comment: *P21, L28 LeVeque (1996). Caps style*

Response: We checked the reference LeVeque (1996) and adapted the capitalization of the title according to the reference style used in The Cryosphere.

Comment: *P22, L15 Nye (1957): Caps style*

Response: We checked the reference Nye (1957) and adapted the capitalization of the title according to the reference style used in The Cryosphere.

Comment: *P22, L35 Ostrem (1959): Caps style*

Response: We checked the reference Östrem (1959) and adapted the capitalization of the title according to the reference style used in The Cryosphere.

2 Response to Anonymous referee #2

We would like to thank Anonymous Referee #2 for detailed and helpful comments on our manuscript.

2.1 General Comments

Comment: *It would be a significant change, and I suggest this as being purely optional, but you may consider moving more of the benchmark results (and the detailed discussion thereof into the supplementary documents). This would serve to focus the paper more on the glaciological applications of the model. I have also made some suggestions below on where you can add more references to relevant field work that shows these types of englacial debris features. Including these may also help broaden this paper and bring it back to a more general glaciology audience.*

Response: We decided not to change the overall structure of the manuscript, as it would take away the focus from the extensive benchmark testing, which we think is an important contribution of this manuscript. Still, we included additional field work references, as suggested in the Specific Comments by Anonymous Referee #2.

Comment: *You go to great lengths to model the change in the concentration of the debris deposit as it is advected. However, all that can be seen from your figures of the 2-D test are the modelled changes in the geometry of the debris deposit. This is too bad, because, (as you say in P3, L7), the basic location and hence changing geometry of the overall debris deposit could be modelled using simple streamlines. What you bring to the table is much more powerful, however. If possible, I suggest changing the color bar / color scheme on the panels of Figure 9 so that the change in concentration as the material is advocated can actually be seen. However, I realize this may be impossible now.*

Response: As a response to this comment, we want to revisit the meaning of changes in concentration in the model results. We present a model which simulates the evolution of the debris concentration field within a glacier. The changes in concentration distribution are currently driven by advection with the glacier flow. As we treat glaciers as incompressible fluids, the resulting glacier flow fields are divergence-free and hence the concentration of debris in a control volume that is advected and deformed by the flow should not change (from a Lagrangian perspective). For a fixed volume in space, the concentration changes, as debris is advected through this fixed volume (from a Eulerian perspective) (see manuscript P3, L23-35 and P3, L26 - P4, L2 in revised manuscript). By modelling the concentration distribution, the model provides the required knowledge to model debris cover formation on the glacier surface due to emergence of englacial debris bands. As a result of the incompressibility assumption, changes in concentration at the edges of the debris inclusions are purely a result of numerical diffusion and mesh resolution and can hence be taken as a key metric of model performance, which we show in the benchmark tests in Sect. 5.1.

On P3, L7 we say that the location of an individual clast (single debris particle or the centre of an "undeformable" boulder) can be calculated by simple streamline tracing. However, the exact location of emergence as well as the transient shape of a polymictic debris inclusion, which will be deformed when advected through a glacier, cannot be recovered by simple streamline calculations. Even more, this becomes exceedingly difficult when the glacier geometry is changing, and hence the velocity fields. In the Specific Comments, we address the comments on the changes in concentration and the use of the color scheme in

Fig. 9 in more detail.

2.2 Specific Comments

Comment: *P1, L18: This is still true for debris covered glacier systems that undergo no melt (cold-based alpine glaciers in Antarctica, for example. See Kowalewski et al. (2011) or Mackay and Marchant (2016). Change "melt " to "ablation "*
Response: We changed "melt" to "ablation".

Comment: *P1, L18: I suggest that you change ". . . and transport of rock. . . " to ". . .or transport of rock. . . " Although it is unusual to find these decoupled, there could be situations, where debris supply is high and yet, due to a significant slope, the transport is so efficient that you never develop a large debris-covered ablation zone.*
Response: The sentence reads: "If debris supply and melting is sufficiently high, and transport of rock material out of the glacier system is inefficient, a debris-covered glacier can develop, where a large portion of the ablation zone is covered with a continuous layer of rock material (Kirkbride, 2011)." The "and transport of rock" implies that in any case, an inefficient transport of rock material out of the glacier system is required to be able to develop a debris-covered glacier, which is also true for the situation mentioned in the comment. Therefore, we chose to leave this sentence as it is.

Comment: *P2, L2-7: Several other authors have suggested / developed this idea as well. You may want to include some additional references. i.e. Ackert (1998); Clark et al. (1998); Monnier and Kinnard (2015); Shroder et al. (2000) and others.*
Response: We now added citations for (Ackert, 1998; Clark et al., 1998) after the sentence that reads: "The implication of this process-continuum is that glaciers can transition between rockglaciers, debris-covered glaciers and clean ice glaciers through space or time as a result of the varying ice influx."

Comment: *P2, L9: Also look at the work of Reznichenko et al. (2011)*
Response: Thanks for this, we added a citation of the work of Reznichenko et al. (2011).

Comment: *P3, L11: Other field studies have shown or inferred this as well. Look at the work of Mackay et al. (2014)*
Response: Thanks for this reference, we added a citation of the work of Mackay et al. (2014).

Comment: *P3, L18: This is a reasonable assumption for this iteration of the model. However, I hope that future models versions may be able to assign spatially heterogeneous rheological properties based on debris concentration.*
Response: From a numerical point of view, it is rather easy to add spatially and temporally heterogeneous rheological properties. An excellent example is given by Aschwanden et al. (2012) with an entropy based rate factor A. Thus if a rheological parametrization based on debris content supported by convincing field data is published in the future, it can be incorporated in

the model framework. However, so far the knowledge on rheological properties of debris-laden ice is limited to a small number of shear tests (e.g. Fitzsimons et al., 2001) and a recent review of available observations and model approaches (Moore, 2014) highlights both the complexity of the rheology of ice-debris mixtures and the need for further laboratory or field testing of models.

Comment: *P5, L23. P6, L1: It is not required, but I suggest you consider moving these sections (3.1 and 3.2) from the main text and putting this information into the supplemental documents. You are mostly describing tools and models that are already published. Unless you have modified them, then you don't really need to describe them here again.*

Response: We thank Anonymous Referee #2 for this suggestion but chose to keep these sections in the manuscript to provide introductory information on the tools that are used to develop the presented model.

Comment: *P6, L33. This adaptive mesh refinement is excellent. Do you also coarsen the mesh behind (upstream) of the deposit once it has transitioned down the streamline?*

Response: Due to the way the mesh refinement is implemented, no mesh coarsening is needed upstream of the advected debris features once they have been transported further downstream. In every refinement time step, the refinement is performed on a mesh that is coarse over the entire domain and only the regions of interest i.e. where debris is present and its surroundings (whose extent depends on the chosen refinement time step and the actual velocity) are refined. As the same domain-wide coarse mesh is used for every refinement time step, the regions further upstream of the actual location of the debris feature, where it has been transported through previously, do not become refined in the subsequent refinement time step any more. This spares the need for mesh coarsening. This is expressed in the manuscript at the end of P6, Sect. 3.3.

Comment: *P7, L11. You did not show results of this "comparison " in this manuscript correct? I think that you mean that in general, the results are similar to those in de Frutos et al. (2014). - which is fine - but the way this sentence is written it sounds like you have actually done the comparison and included them in your results here. For clarity, I suggest that you change the sentence slightly to read: "Comparing Results of the benchmark test in Sec 5.1 derived with our approach compare well with adaptive mesh refinement based on a posteriori error estimation (de Frutos et al., 2014), and demonstrate that ...".*

Response: This is correct, thanks. We changed the sentence to: "The results of the benchmark test in Sec. 5.1 derived with our approach compare well with that derived using adaptive mesh refinement based on *a posteriori* error estimation (de Frutos et al., 2014), this demonstrates that ...".

Comment: *P9, L21: Define uh, ue and L2 in the equation*

Response: We inserted the definitions by changing the relevant sentence to: "In order to evaluate the chosen cell area threshold, we perform convergence tests where (a) $\|c_\mathrm{h} - c_\mathrm{e}\|_{\mathrm{L}_2} = \sqrt{\sum_{k=1}^{n}(c_{\mathrm{h}_\mathrm{k}} - c_{\mathrm{e}_\mathrm{k}})^2}$ the L2 norm of the error between the computed finite element solution c_h and the exact solution c_e, where n is the number of computation locations, and (b) the Root Mean Square (RMS) error between the computed finite element solution and the exact solution for different cell size thresholds are

computed. Therefore, we first compute the exact solution on the same mesh that is used in the finite element solution."

Comment: *P9, L26: here you have defined T as total time. I do not think that that is what you are using for T in equations (1a) and P4, L18.*

Response: In P4, L18 T is used to describe the transpose of the respective quantity. For clarity we altered it to $\top$. We also adjusted the text to use t_{total} instead of T to describe the total time.

Comment: *P10, L2: It is interesting that you choose a value for A that is best suited to temperate glaciers, but then use a no-slip boundary condition at the glacier-bed interface. I understand the no-slip boundary for these tests, but this condition is more consistent with cold-based polar glaciers which would have colder ice and a different value of A.*

Response: For these tests, the choice of the exact numerical value for A is not critical, as we were not trying to reproduce the actual debris transport of Haute Glacier d'Arolla, but to show the general features of debris transport within mountain glaciers. The choice of a smaller constant value of A, representative for cold-based glaciers and consistent with a "real world" no-slip boundary condition, would only cause a reduction of glacier flow velocities but not change the actual velocity patterns (see Fig. 1). This would increase the amount of time needed to transport the debris deposits downglacier, but would not induce a change of the main features and characteristics of the transport and associated deformation of debris inclusions observed in the tests. In future applications of the model, where we are planning to simulate the evolution of specific debris-covered glaciers, we will apply site-specific basal conditions and appropriate flow law parameters representative for the thermal regime of the glacier. For clarity, we rephrased the first sentence of Sect. 4.2 to: "The purpose of these tests is to demonstrate the characteristics of debris transport within mountain glaciers, not to reproduce a particular event on a specific glacier. Hence, all velocity computations are initialized with a no-slip condition at the glacier/bedrock boundary, the flow law exponent n is set to 3 and the Glen rate factor A is set to $2.4 \times 10^{-24}\ \mathrm{s}^{-1}\mathrm{Pa}^{-3}$, a standard value for temperate ice (Cuffey and Paterson, 2010)."

Comment: *P10, L27: Remove sentence beginning: "Thereby, analysis of. . . " This sentence is unnecessary.*

Response: This sentence aims to explain the chosen test setup, therefore we kept it in the revised manuscript but changed it to: "These debris deposits of varying size, shape and location of deposition were chosen to facilitate analysis of the interplay between debris input location, deformation during transport and the zone of emergence."

Comment: *P11, L9: How big of a "bump " did you put in the subglacial topography? The reader has no way of knowing the characteristics of this or any other subsurface features based on the information and figures shown (see also my comment on Figure 5). Without this knowledge we cannot evaluate the impact (which I suspect is very little) that this should have on the simulation results.*

Response: We adjusted Fig. 5 to illustrate the subglacial topography of the idealized 3D glacier case.

Comment: *P13, L7: You describe the results of the rotational flow test (Fig 6) in great detail, but then barely mention the*

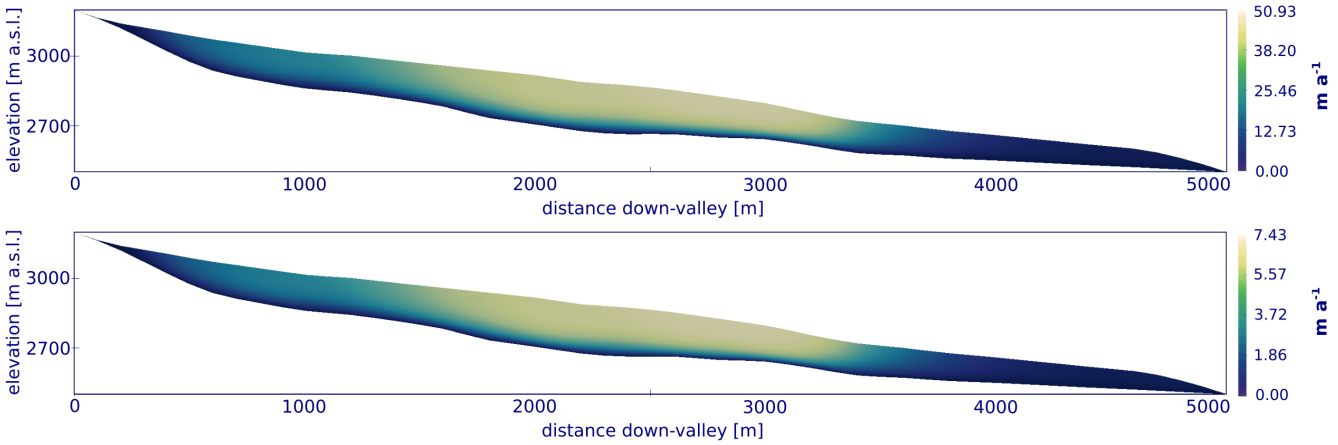

Figure 1. Velocity of 2D glacier profile. (a) temperate conditions with $A = 2.4 \times 10^{-24}\ \mathrm{s}^{-1}\mathrm{Pa}^{-3}$, standard value for temperate ice (Cuffey and Paterson, 2010) and (b) cold-based conditions with $A = 3.5 \times 10^{-25}\ \mathrm{s}^{-1}\mathrm{Pa}^{-3}$ a value for cold ice at roughly -10 degrees Celsius (Cuffey and Paterson, 2010)

.

swirling flow case (Figure 7). Is there a reason for this? In any case, I suggest that you move the swirling flow case (Fig. 7) to the Sup docs.

Response: The swirling flow test is identical to the "rotating three body problem" but using a different velocity field, which forces the features to first change their shape but then recover their initial shape at total time $t = 1.5$ s. Hence, this offers an even more challenging test case for the advection module and we included the figure to demonstrate that our model is as well capable of producing appropriate results in this test. Since the test cases are identical except the velocity field used, we keep the description short but we now changed the sentence on P13, L7 (P13, L2 in revised manuscript) to: "Also, when the initial concentration pattern is subjected to a more complex, swirling flow (LeVeque, 1996), the results of these more challenging test simulations again show satisfactory model performance, as can be seen in Fig. 7 and Fig. A5 in the supplementary material." (Fig. 7 and Fig. A6, in revised manuscript)

Comment: *P15, L24-25: It is too bad that you did not show results from these simulations (using layer-shaped features). Although the sphere test is interesting, the layer deposits are more applicable to glaciological problems and questions. Perhaps these results were too difficult to visualize in 3D?*

Response: We are aware of the glaciological relevance of layer deposit simulations, however we chose to not present initial layer results at this stage as they deserve a detailed discussion and would be more informative if they were based on a real world example. We plan to perform such a study in the near future.

Comment: *P17, L1-3: It would be helpful if you include a reference as examples of instances where this has been the as-*

sumption.

Response: We included a reference of the work of Naito et al. (2000), where this assumption has been made.

Comment: *P17, L1-13: It is interesting in this discussion that you have not emphasized the importance of also of now being able to quantify the changes in the debris concentration as it moves and deforms down-glacier. I would mention this. Although out of scope of this study, determining the rate of debris cover formation in the ablation zone (which is one of the main potential applications of this model once it is linked to an ablation model) is directly linked to the debris concentration and thickness of the emerging debris bands. Your model allows this to now be predicted.*

Response: The current study focuses on demonstrating a numerically stable advection scheme that can be used to predict transport and deformation of debris features, as Anonymous Referee #2 points out above. However when looking at "local" debris concentrations and their potential change over time, one has to be careful to describe the reference frame in which these changes take place. From a fluid dynamics point of view, the concentration of debris in a control volume that is advected and deformed by the flow should not change when the fluid is incompressible. This is described in the manuscript on P3, L23-35. We currently focus on that property of the model as it demonstrates the performance of our numerical implementation when we assume D, the debris diffusivity, to be very small, or even zero, and thus advection being the dominant transport process. In contrast to this Lagrangian viewpoint, a more applied (even Eulerian) viewpoint would be to investigate a fixed volume in space and time. In this case, debris concentration changes over time and such changes are very interesting for the interaction of debris with mass balance processes or the formation of emerging debris bands, as Anonymous Referee #2 points out above. We have added a sentence to the manuscript to highlight this potential application in future studies: "The model presented here allows us to simulate the advection of debris concentration through a glacier in great detail and therefore any resulting local concentration changes (Eulerian perspective), e.g. the deformation of debris deposit shape (Lagrangian perspective, cf. Fig. 10)."

Comment: *P17, L7-12: I'd would also recommend that you take a look at the work of Mackay and Marchant (2017) where englacial debris layers are directly linked to modelled changes in the environmental conditions in the accumulation zone (at orbitally-paced time scales). Mentioning that being able to test theories like this and similar shows another area in which your model can be very useful and adding this into the discussion would broaden the perceived applicability of your work.*

Response: Thanks for this reference. We included the following sentence at the end of Sect. 6.1: "This model also offers the possibility to test the findings of studies that use patterns of englacial debris distribution on Antarctic debris-covered glaciers to infer climate information at orbitally-paced time scales (Mackay and Marchant, 2017)."

Comment: *P18, L1-2: How hard would it be to implement a debris concentration - dependent rheology into your modelling framework? This would be excellent to have in future iterations of the model. See similar comment above.*

Response: In principle, the implementation would be rather simple. Compare comment above.

2.3 Technical Corrections

We thank Anonymous Referee #2 for the detailed Technical Corrections suggested for the text of the manuscript.

Comment: *P1, L4: Change "As debris is. . . " to "Because debris is. . . "*
Response: Done.

Comment: *P1, L6: Change ". . .surface requires that the englacial transport pathways and deformation can be known. " to ". . .surface requires knowledge of the englacial transport pathways and deformation. "*
Response: Done.

Comment: *P2. L13: Change ". . .get the full. . . " to ". . .model the full. . . "*
Response: Done.

Comment: *P2. L17: Add comma ". . . Anderson, 2016), but as. . . "*
Response: Done.

Comment: *P3. L25: Remove: " as incompressibility enforces conservation of ice density and hence ice volume. " this clause is not necessary.*
Response: We now rewrite the sentence as follows: "Assuming that ice is an incompressible fluid, and consequently that the ice flow fields must be divergence-free, any deformational patterns inducing horizontal elongation, must, at the same time, cause vertical compression. In the context of englacial debris transport, this implies that the initial debris concentration is constant for an initial control volume of ice being tracked (i.e. seen from Lagrangian perspective)."

Comment: *P3, L29: Start a new paragraph at the sentence "To solve the . . . "*
Response: We started a new paragraph at P3, L23 (P3, L26 in revised manuscript) instead of L29 as this is one block of information.

Comment: *P3, L35: Consider deleting or moving the rest of this paragraph starting with the sentence: "In a later stage. . . " This information is better suited to the "Conclusions and outlook " section at the very end of the paper.*
Response: We included this sentence in the Introduction to clarify the scope of this paper, but also the context in which we are developing this model. We changed the sentence to: "The model presented here forms part of an envisaged fully-integrated model framework that, by including (1) a free-surface evolution scheme including debris-aware mass balance subroutines and

(2) a transport model for debris at the glacier surface interacting with the mass balance subroutines, will be capable of simulating the transient response of debris-covered glaciers, with predetermined debris inputs, to a changing climate."

Comment: *P4, L6, L7: Be consistent with using either "Section " or "Sec. "*

Response: We replaced "Section" and "Sec." with "Sect." following the guidelines for manuscript preparation of The Cryosphere.

Comment: *P4, eqn. (1a) and P4, L18: define "T " somewhere*

Response: We have changed "T" to the symbol "$\top$" as a more appropriate symbol to express that a quantity has been transposed.

Comment: *P5, eqn. (5b): define $\partial\Omega_{\mathrm{D}}$. I assume that this is supposed to be $\partial\Omega_{\mathrm{bed}}$. If not, then unless D is for the diffusion coefficient, choose another notation.*

Response: We changed $\partial\Omega_{\mathrm{D}}$ to $\partial\Omega_0$ as in this case it is used to describe the boundary of the entire domain, except where input locations are prescribed. We also included the following sentence in Sect. 4.2 to describe what boundary conditions are used in the glacier tests in this study: "In the presented glacier simulations, all debris inclusions have been deposited in a single event, hence they are all initialized as inclusions within the glacier, i.e. the entire glacier/atmosphere boundary belongs to Ω_0."

Comment: *P6, L19: At sentence: "For 2D simulations. . . " Start new paragraph?*

Comment: *P6, L26: At sentence: "For 3D simulations. . . " Start new paragraph?*

Response: We start a new paragraph at the sentence: "For 2D simulations..", but as some of the concluding sentences correspond to both, the 2D and 3D implementations of mesh refinement, we keep the detailed descriptions of the 2D and 3D case in one paragraph.

Comment: *P6, L27: You have not yet introduced the refinement time step and thus this is confusing. I suggest ending the sentence with a reference to section 3.4. I.e.: ". . .at every refinement time step (see Sec. 3.4). "*

Response: We added the reference to Sect. 3.5 (as we switched Sect. 3.4 and 3.5) at P6, L18 (P6, L20 in revised manuscript) where we first introduce the refinement time step.

Comment: *P7, L2: This sentence is awkward and should be reworded.*

Response: We changed the sentence to: "Adaptive mesh refinement strategies often employ *a posteriori* error estimation (e.g. John, 2000). The PDE is solved and the assigned error estimators and indicators are used to mark the cells for refinement and potentially coarsening. Subsequently, the marked cells become modified and the PDE is solved on the newly refined mesh. This process is repeated until the error estimators and indicators fall below a user-defined tolerance within every cell."

Comment: *P7, L15: Switch the order of sections 3.4 and 3.5. This improves readability and otherwise the reader does not know what SUPG is when you introduce it in P8, L3.*

Response: Done.

Comment: *P9, L19: Reword the sentence starting with "Here, we. . . " It does not make sense as written.*
Response: We changed the sentence to: "Here, we present results of computations using two different refinement time steps, (a) small refinement time step of $0.01\,\pi$ s and (b) a larger refinement time step of $0.1\,\pi$ s."

Comment: *P12, L9: Edit this sentence for better clarity. I suggest: "The results of benchmark tests 1 and 2 following the Bochev et al. (2004) are shown in . . . "*
Response: We wanted to use the same naming convention as in the original paper (Example 1 and 2), so we now changed the sentence to read: "Our results of reproducing Examples 1 and 2 in the numerical results of (Bochev et al., 2004)...".

Comment: *P12, L13: delete ", exemplary "*
Response: Done.

Comment: *P12, L16: You refer to the case of both refinement time steps. However, so far you have only talked about the single time step (*$0.1\,\pi$*) that is used in Figure 6. I know that you are also talking about the* $0.01\,\pi$ *time step (shown in the sup docs), but it is not clear the way it is written right now. Please edit for clarity.*
Response: We changed the sentence to: "The shapes of the concentration features are well recovered in the case of both refinement time steps (see Fig. 6b for refinement time step $0.1\,\pi$ s and Fig. A4b in the supplementary material for refinement time step $0.01\,\pi$ s)." (Fig. A5b in revised manuscript)

Comment: *P15, L22: change ". . .glacier is becoming narrower. . . " to ". . .glacier becomes narrower. . . "*
Response: Done.

Comment: *P16, L1-3: This sentence is too long and confusing and needs to be edited. I suggest deleting the unnecessary extra qualifiers: ". . .that uniformly cover wider portions of the accumulation area. . . " and "resulting in thick debris deposit but limited in area. . . "*
Response: We edited the sentence, it now reads: "In these simulations, ash fall or avalanche events that uniformly cover wider portions of the accumulation area are included as layer-shaped debris deposits at the glacier surface. Rockfall events that result in a locally thick debris deposit are represented by a circular inclusion, as a possible remnant thereof. Both distinctly different debris inputs become severely elongated and band-like shaped during transport."

Comment: *P16, L2: Change ". . .inclusion as a possible. . . " to ". . .inclusion representative of a possible. . . "*
Response: This sentence has been changed, compare previous comment.

Comment: *P18, L15: change start of line to . . . "that is as course as possible. . .*
Response: Done.

Comment: *P18, L27: Start a new paragraph at this sentence.*
Response: Done.

2.4 Figure Comments

We thank Anonymous Referee #2 for helpful comments to increase the comprehensibility of the figures. If there was more than one comment concerning the same figure, we labelled the referee's comments to be able to address them point by point.

Comment: *Figure 1: Include a north arrow and scale bar*
Response: Done.

Comment: *Figure 3: - Please mark the ELA / beginning of the ablation zone. Although the reader can infer this from where the vertical velocity component passes zero from negative to positive, the addition of a simple arrow or line would be appreciated and aid in interpretation of Figure 9.*
Response: As these glacier cases are based on fixed velocity fields (based on Eq. 1 in the manuscript and given glacier geometries) and are not connected to a mass balance routine, inclusion of an ELA marker could be misleading. We added a contour line of zero vertical velocity.

After contemplating the term "steady-state" as it has been used in the manuscript and the comment of Anonymous Referee #2 above, we came to the conclusion that the term is misleading in the absence of a mass balance model in our current study. Thus the term has been replaced with "fixed velocity field" in the manuscript.

Comment: *Figures 3 and 4: - Since this geometry represents a glacier, but I suggest that you label x-axis and y-axis accordingly. i.e, "distance (m) " and "elevation (msl)*
Response: We labelled the x-axis with "distance down-valley [m]" and the y-axis with elevation [m a.s.l.].

Comment: *Figure 5:*
1. I'm not sure why you have rotated the view individual panels unless you are trying to show the overall geometry. If this is the case, then it is not effective but rather just makes the figure look rather messy and less clear. It is not required, but if possible, I suggest that you show all output in the same orientation.
2. Rather than using the axis labels x-axis, y-axis z-axis, consider using the physical interpretations for the labels (i.e. elevation, distance down-valley, distance cross-valley)

3. A wireframe showing just the glacial bed would be appreciated. As it is now, the reader has no way of knowing what the subglacial topography looks like or where the bedrock "hump " is located.

4. This is out of main scope of the debris transport focus of the paper, but I am curious as to why there is such a pronounced positive vertical velocity component at the upper right side of the glacier near the valley bend. There is compressive strain encouraging the emergence of ice here, but the magnitude surprises me.

Response: 1. We now show all output in the same orientation and for clarity added two further panels. Panel (d) shows a 2D down-valley projection of the central flowline and panel (e) shows the underlying bed geometry.

2. Done.

3. We added this as panel (e) .

4. This high compressive strain region which creates rather large but not unrealistic vertical velocities is a result of solving Eq. 1 (manuscript) for our assumed glacier geometry.

Comment: *Figure 6: - The figure is fine. The caption could use some style adjustments for readability.*

1. In this and all figure captions where you have separate panels, you do not need to use the phrase: "In (a) etc. . ...is shown " Just start with the intended panel letter and say what it is as a separate sentence.

2. Remove the sentence: "The data ranges from -0.14 *to* 1.11*. " We can see that from the figures.*

3. Move the sentence "Color scales show concentration values " to the beginning or end of the caption.

4. Shorten the final sentence to: (f) Results of the convergence test as a function of mesh refinement parameter cvol.

Response: 1. Done.

2. Done.

3. Done.

4. Done.

Comment: *Figure 7 caption:*

- Same style change comments as for figure 6.

Response: Done.

Comment: *Figure 8:*

- The first two panels fail to convey the intended information. I think that there are two separate surfaces represented for each contour (except 90) when I zoom way in, but it is barely possible to resolve these as separate at the print level of figure zoom. Also, which surface is the FEM solution and which is the analytical? These are the same color and are not labeled or marked. I recognize that they are basically the same – which may be the point of the figure, but as it is now, it is just unclear. I suggest removing the panels (a) and (b) and just leaving in panel (c) which does convey usable information.

Response: In this figure, we intended to provide a visual comparison between the FEM and the analytical solution as an additional means of illustrating the model performance. We now adjusted the figure so that the contour lines of the FEM solution

and the analytical solution can better be distinguished from each other, by showing the analytical solution in solid grey and only the computed FEM solution in color and adjusted the figure caption accordingly, to highlight our intent with panels (a) and (b).

Comment: *Figure 9:*

1. The color scale (red gradient) for concentration is not effective at conveying any information as all the lines basically look like the same shade of red. It may be impossible now, but if possible, consider changing this to a multiple-color colors scheme so that the change in concentration can actually be seen.

2. Panels (a-c): Label the x-axis ('distance down-valley (m)). You probably only need to do this once for all panels.

3. Label (draw an arrow or something) the various debris layers (D1, D2, D3, etc.). Right now, it is not possible to track which is which layer.

4. Why not label the actual panel somewhere with their simulation times (24 yrs, 62 yrs, 85 yrs)

5. Panel (d): label the x and y-axis correctly and put in at least two number values on each of the axes. Otherwise, the reader has no idea of the spatial scale.

6. Why not label the actual panels with their simulation times (0.2 yrs, 8, yrs, 20 yrs, 26 yrs)

7. Caption: Remove unnecessary sentence: "Concentrations are displayed in the range of 0 to 100. " You already show this on the color scale.

Response: 1. The concentration changes at the edges of the features are based on numerical diffusion only, which is well controlled, as demonstrated by our benchmark experiments and can be nicely seen in the cross-sections of Fig. 8c. Thus changing to a multiple-colors color scheme only creates very colorful edges but does not convey the results better and we consider it as visually less appealing (Fig. 2). As concentration is given as a continuous function and we do not want to introduce subjective categories, we want to keep a sequential color scheme instead of a qualitative color scheme.

2. Done.

3. We labelled all the present debris inclusions.

4. Done.

5. Done.

6. Done.

7. As we do not want to misleadingly claim that our results have no numerical oscillations we wish to retain this sentence, but now rephrase it as: "Numerical oscillations as excursions beyond the initial values of 0 or 100 are of magnitude less than ± 17 and are truncated to the data limits".

Comment: *Figure 10:*

1. A rough 2-d outline of the glacier (surface, bedrock along the centerline in the x-z plane and the glacier sides in the x-y plane) would be helpful for interpretation. This does not have to be exact. Please label the axis relative to the glacier model (i.e. elevation, distance down-valley, distance cross-valley)

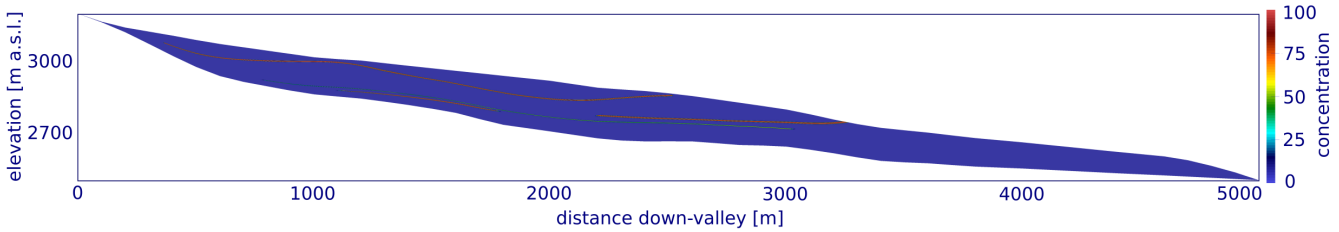

Figure 2. Results of the debris transport simulations for the 2D longprofile of Haute Glacier d'Arolla for a multiple-colors color scheme (cf. Fig.9 in the manuscript). Debris concentration at 62 years after start of the simulations is shown. Concentrations are displayed in the range of 0 to 100, numerical oscillations as excursions beyond the initial values of 0 or 100 are of magnitude less than ±17 and are truncated to the data limits.

.

2. Label the debris distributions with their simulation times directly on the figure. There is plenty of room and this would make interpretation easier.

3. Caption: Remove unnecessary sentence: "Concentrations are displayed in the range of 0 to 100. " You already show this on the color scale.

Response: 1. We labelled the axes as suggested and added the glacier body in a transparent style in order to help to visually locate the debris inclusions.

2. Done.

3. As we do not want to misleadingly claim that our results have no numerical oscillations we wish to retain this sentence, but now rephrase it as: "Numerical oscillations as excursions beyond the initial values of 0 or 100 are of magnitude less than ± 4 and are truncated to the data limits".

2.5 Supplementary Material Comments

Comment: *This may be a problem with my video player (I tried several) or my download, but I cannot play some of the .avi movie files. Please check that these are not damaged.*

These play successfully:

3d_benchmark1.avi

2d_glaciercase.avi

These do not load (error):

2d_benchmark_exp1t20.avi

2d_benchmark_exp1t200.avi

2d_benchmark_exp2t15.avi

2d_benchmark_exp2t150.avi

Response: We could successfully play all the downloaded videos with the following players on different operating systems:
Ubuntu: VLC media player
Windows 7: VLC media player, Quicktime, Windows media player
macOS Sierra: VLC media player, Quicktime

Comment: *Figure A1:*
1. Please put a scale or tick marks on the x-axis and y-axis. the reader ha no idea what the scale is. Or is this dimensionless?
2. Label the color bar in panels (a) and (b).
3. In panel (b), if all the velocities are the same, then state that in the caption. Putting the "1.22 " beneath the panel looks strange and does not convey any useful information.

Response: 1. We added in the text as well as the figure caption that the computations are performed and the data in the plots is shown for the unit square ($1\ \mathrm{m} \times 1\ \mathrm{m}$).
2. Done.
3. Done.

Comment: *Figure A2 and A3:*
1. Label the panels in the left hand column (2D concentrations) with the dt used in that row. The left hand panels need x-axis and y-axis labels/tick marks (0 – 1?), otherwise the reader has no way of knowing where the profiles in the middle and right hand panels are taken from. You may also want to put two dashed lines across the concentration panels that show the location of the profiles.
2. It is odd that you put your References section in the middle of the document before Figure A2. Maybe this is something that happened in the auto-collate process during submission? I suggest just moving all Sup Doc references to the end of the document.

Response: 1. We labelled the axes and included lines to indicate the location of the right hand side profiles in the concentration plots. In order to prevent the figures from being crowded, we skipped the dt as a label.
2. Done.

References

Ackert, Jr., R. P.: A rock glacier/debris-covered glacier system at Galena Creek, Absaroka Mountains, Wyoming, Geogr. Ann. A, 80, 267–276, doi:10.1111/j.0435-3676.1998.00042.x, 1998.

Aschwanden, A., Bueler, E., Khroulev, C., and Blatter, H.: An enthalpy formulation for glaciers and ice sheets, J. Glaciol., 58, 441–457, 2012.

Bochev, P. B., Gunzburger, M. D., and Shadid, J. N.: Stability of the SUPG finite element method for transient advection–diffusion problems, Comput. Method. Appl. M., 193, 2301–2323, doi:10.1016/j.cma.2004.01.026, 2004.

Bozhinskiy, A., Krass, M., and Popovnin, V.: Role of debris cover in the thermal physics of glaciers, J. Glaciol., 32, 255–266, 1986.

Clark, D. H., Steig, E. J., Potter, Jr., N., and Gillespie, A. R.: Genetic variability of rock glaciers, Geogr. Ann. A, 80, 175–182, doi:10.1111/j.0435-3676.1998.00035.x, 1998.

Cuffey, K. M. and Paterson, W. S. B.: The Physics of Glaciers, Academic Press, Burlington, MA, 4th edn., 2010.

de Frutos, J., García-Archilla, B., John, V., and Novo, J.: An adaptive SUPG method for evolutionary convection–diffusion equations, Comput. Method. Appl. M., 273, 219–237, doi:10.1016/j.cma.2014.01.022, 2014.

Fitzsimons, S. J., McManus, K. J., Sirota, P., and Lorrain, R. D.: Direct shear tests of materials from a cold glacier: implications for landform development, Quatern. Intern., 86, 129–137, 2001.

Glen, J. W.: The creep of polycrystalline ice, Proceedings of the Royal Society of London A: Mathematical, Physical and Engineering Sciences, 228, 519–538, doi:10.1098/rspa.1955.0066, 1955.

John, V.: A numerical study of a posteriori error estimators for convection–diffusion equations, Comput. Method. Appl. M., 190, 757–781, doi:10.1016/S0045-7825(99)00440-5, 2000.

John, V. and Novo, J.: Error analysis of the SUPG finite element discretization of evolutionary convection-diffusion-reaction equations, SIAM J. Numer. A., 49, 1149–1176, doi:10.1137/100789002, 2011.

Kirkbride, M. P.: Debris-Covered Glaciers, in: Encyclopedia of Snow, Ice and Glaciers, edited by Singh, V. P., Singh, P., and Haritashya, U. K., pp. 180–182, Springer Netherlands, Dordrecht, 2011.

Kowalewski, D. E., Marchant, D. R., Swanger, K. M., and Head, J. W.: Modeling vapor diffusion within cold and dry supraglacial tills of Antarctica: Implications for the preservation of ancient ice, Geomorphology, 126, 159–173, doi:10.1016/j.geomorph.2010.11.001, 2011.

LeVeque, R.: High-resolution conservative algorithms for advection in incompressible flow, SIAM J. Numer. A., 33, 627–665, doi:10.1137/0733033, 1996.

Mackay, S. L. and Marchant, D. R.: Dating buried glacier ice using cosmogenic ^{3}He in surface clasts: Theory and application to Mullins Glacier, Antarctica, Quaternary Sci. Rev., 140, 75–100, doi:10.1016/j.quascirev.2016.03.013, 2016.

Mackay, S. L. and Marchant, D. R.: Obliquity-paced climate change recorded in Antarctic debris-covered glaciers, Nat. Commun., 8, 14 194, doi:10.1038/ncomms14194, 2017.

Mackay, S. L., Marchant, D. R., Lamp, J. L., and Head, J. W.: Cold-based debris-covered glaciers: Evaluating their potential as climate archives through studies of ground-penetrating radar and surface morphology, J. Geophys. Res.-Earth, 119, doi:10.1002/2014JF003178, 2014.

Monnier, S. and Kinnard, C.: Reconsidering the glacier to rock glacier transformation problem: New insights from the central Andes of Chile, Geomorphology, 238, 47–55, doi:10.1016/j.geomorph.2015.02.025, 2015.

Moore, P. L.: Deformation of debris-ice mixtures, Rev. Geophys., 52, 435–467, doi:10.1002/2014RG000453, 2014.

Naito, N., Nakawo, M., Kadota, T., and Raymond, C. F.: Numerical simulation of recent shrinkage of Khumbu glacier, Nepal Himalayas, Proceedings of an International Workshop Held at the University of Washington in Seattle, Washington, USA, 13–15 September 2000, IAHS Publication, 264, 245–254, 2000.

Nye, J. F.: The distribution of stress and velocity in glaciers and ice-sheets, Proceedings of the Royal Society of London A: Mathematical, Physical and Engineering Sciences, 239, 113–133, doi:10.1098/rspa.1957.0026, 1957.

Reznichenko, N. V., Davies, T. R., and Alexander, D. J.: Effects of rock avalanches on glacier behaviour and moraine formation, Geomorphology, 132, 327–338, doi:10.1016/j.geomorph.2011.05.019, 2011.

Shroder, J. F., Bishop, M. P., Copland, L., and Sloan, V. F.: Debris-covered glaciers and rock glaciers in the Nanga Parbat Himalaya, Pakistan, Geogr. Ann. A, 82, 17–31, 2000.

Östrem, G.: Ice melting under a thin layer of moraine, and the existence of ice cores in the moraine ridges, Geogr. Ann., 41, 228–230, 1959.

Modelling debris transport within glaciers by advection in a full-Stokes ice flow model

Anna Wirbel[1], Alexander Helmut Jarosch[2], and Lindsey Nicholson[1]

[1]Institute of Atmospheric and Cryospheric Sciences, University of Innsbruck, Innsbruck, Austria
[2]Institute of Earth Sciences, University of Iceland, Reykjavík, Iceland

Abstract. Glaciers with extensive surface debris cover respond differently to climate forcing than those without supraglacial debris. In order to include debris-covered glaciers in projections of glaciogenic runoff and sea-level rise, and to understand the paleoclimate proxy recorded by such glaciers it is necessary to understand the manner and timescales over which a supraglacial debris cover develops. ~~As~~ Because debris is delivered to the glacier by processes that are heterogeneous in space and time, and these debris inclusions are altered during englacial transport through the glacier system, correctly determining where, when, and how much, debris is delivered to the glacier surface requires ~~that the~~ knowledge of englacial transport pathways and deformation~~can be known~~. To achieve this, we present a model of englacial debris transport in which we couple an advection scheme to a full-Stokes ice flow model. The model performs well in numerical benchmark tests, and we present both 2D and 3D ~~steady-state~~ glacier test cases that, for a set of prescribed debris inputs, reproduce the englacial features, deformation thereof, and patterns of surface emergence predicted by theory and observations of structural glaciology. In a future step, coupling this model to a (i) debris-aware surface mass-balance scheme and (ii) supraglacial debris transport scheme will enable the co-evolution of debris-cover and glacier geometry to be modelled.

1 Introduction

All mountain glaciers carry rock and dust material within the ice. This can originate from gravitational mass movements from the surrounding valley walls, aeolian deposition, or basal erosion (Benn and Evans, 2010). Rock and dust debris deposited onto the surface of a glacier in the accumulation zone is buried by subsequent snowfall and transported englacially with the glacier ice as it flows downslope. In the ablation zone of a glacier, ice flow transports debris towards the glacier surface and surface ice ablation leaves behind a residue of rock material (Fig. 1a). If debris supply and ~~melting~~ ablation is sufficiently high, and transport of rock material out of the glacier system is inefficient, a debris-covered glacier can develop, where a large portion of the ablation zone is covered with a continuous layer of rock material (Kirkbride, 2011).

A surface debris cover more than a few centimeters thick inhibits surface ablation of ice and thus alters glacier runoff, local water resources and contribution to sea level change. It also affects glacier dynamics and geometry such that low-angled, stagnating debris-covered ice can survive for longer at lower altitudes than neighbouring clean ice glaciers (Benn et al., 2012; Anderson and Anderson, 2016). Thus the paleoclimatic signal represented by sediment deposits from a debris covered-glacier is not the same as one from a clean ice glacier.

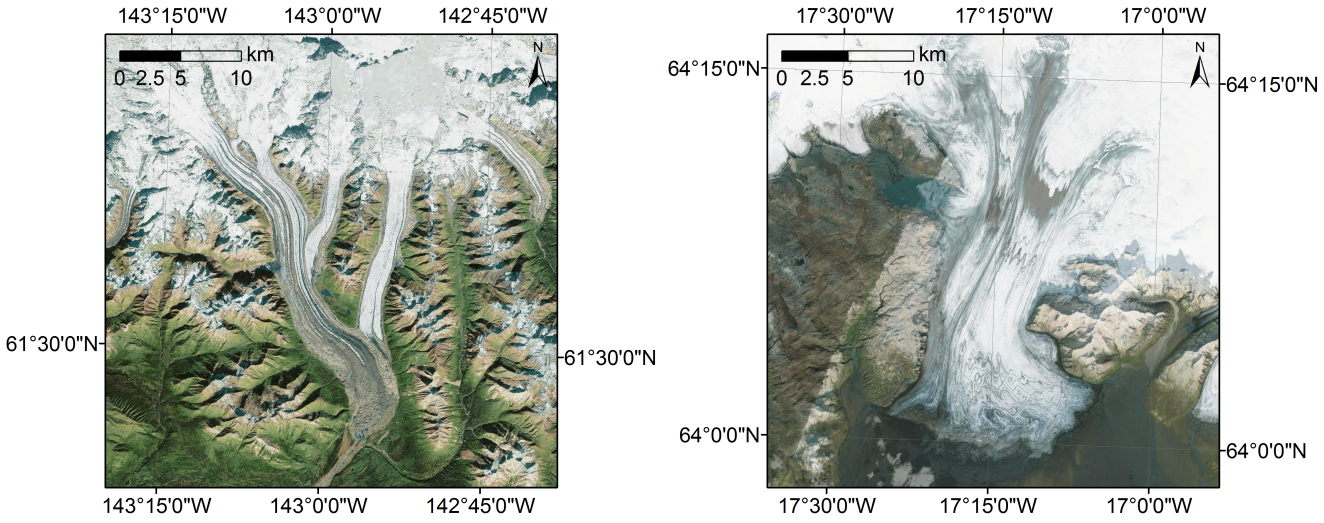

Figure 1. (a) Debris-covered ~~Kennikott~~ Kennicott Glacier, Wrangell Mountains, Alaska, USA and (b) deformed englacial bands emerging at the surface of Skeiðarárjökull, an outlet glacier of Vatnajökull ice cap, Iceland. Source: ESRI basemap DigitalGlobe ~~(a) 21/6/2015 and (b) 5/6/2013~~ imagery .

Fluxes of ice and debris change over time in response to climatic variations, and in space due to differences in local site characteristics. Kirkbride (1989) proposes that variations in ice mass influx serve to unify a process-continuum of deformational geomorphological features of mixed ice and debris composition. The implication of this process-continuum is that glaciers can transition between rockglaciers, debris-covered glaciers and clean ice glaciers through space or time as a result of the varying ice influx (Kirkbride, 1989; Ackert, 1998; Clark et al., 1998). Accordingly, the extent of a debris cover varies inversely with the glacier mass balance, whereby the debris cover extent is governed by transport dominant conditions (higher ice velocities and lower surface ablation) during periods of positive mass balance and ablation dominant conditions (lower ice velocities and higher ablation) during periods of negative mass balance (Kirkbride, 2000). In addition, debris covers can be formed instantaneously by isolated events such as ash fall or a large rockfall onto the glacier ablation zone (e.g. Nield et al., 2013; Hewitt, 2009; Shugar et al., 2012), (Reznichenko et al., 2011). The complex interplay between debris supply and ice supply and their variation in space and time mean that the thickness and character of the debris cover, and its resultant impact on the glacier behaviour is also strongly space and time-dependent. In order to resolve this, it is necessary to understand how the debris co-evolves with the glacier. This requires tackling many component parts to ~~get~~ model the full debris-covered glacier system. To date, existing numerical models of debris-covered glaciers either restrict debris inputs to the ablation zone (Konrad and Humphrey, 2000; Menounos et al., 2013; Vacco et al., 2010), prescribe an englacial debris concentration (Bozhinskiy

et al., 1986) or use empirical relationships to describe accumulation of debris on the glacier surface (Jouvet et al., 2011). Recent studies apply simplified treatment of englacial transport (Rowan et al., 2015; Anderson and Anderson, 2016), but as yet, no model explicitly resolves full 3D (three-dimensional), time evolving transport of debris within the ice flow field of the glacier body. This is a significant omission because, as surface debris mainly originates from localized debris inputs (rockfall or mixed avalanche events) in the accumulation zone, modelling englacial transport is crucial to predict the location and timing of surface emergence of debris, as well as its concentration and its spatial extent, all of which are required to constrain the nature of the developing debris cover and its resultant impact on glacier behaviour.

Prevailing stress conditions, and the resulting strain and velocity fields, control sediment transport within an ice body. Individual clasts are considered to be predominantly passively transported by glacier ice, unless within the basal traction zone, and so their shape remains fundamentally unaltered by transport. For a static velocity field, the pathway of such a feature is identical to a streamline within the glacier, but with the evolving glacier geometry these will change. However, debris inputs from rock, mixed snow/ice avalanches and other gravitational mass movements tend to be deposited as bodies of polymictic ice-sediment mixtures, which become severely deformed in the course of transport through the glacier, as revealed by studies of structural glaciology (e.g. Fig. 1b, Jennings et al., 2014), (Mackay et al., 2014). Hence, the initial shape of the deposit will be changed significantly, and this englacial deformation will affect the pattern of debris emergence at the glacier surface (e.g. Goodsell et al., 2005). In order to numerically model transport and deformation of sediment inclusions, a full representation of 3D velocity fields resolving all spatial gradients is essential, which calls for a full-Stokes ice flow modelling approach.

Here we present a new model that simulates transport, and resultant deformation, of material within a glacier coupled to 3D resolved ice flow, and we demonstrate the capabilities and performance of the model through a series of evaluation simulations. Although dynamics of debris-ice mixtures can differ from clean ice dynamics depending on several parameters such as concentration of debris, particle size and temperature (Moore, 2014), in this work we assume that sediment inclusions within the glacier do not affect ice rheology due to the small total amount of transported material in comparison to overall ice volume. The model is coded in python and relies on the FEniCS framework, an open-source software for automated solution of partial differential equations (Alnæs et al., 2015; Logg et al., 2012a). The model employs an existing benchmarked full-Stokes ice flow model (*icetools*, Jarosch, 2008, now implemented in FEniCS) to compute 3D velocity fields that govern an advection algorithm used to describe debris transport.

Assuming that ice is an incompressible fluid, and consequently that the ice flow fields must be divergence-free~~. As a consequence~~, any deformational patterns inducing horizontal elongation, must, at the same time, ~~have to~~ cause vertical compression~~, as incompressibility enforces conservation of ice density and hence ice volume~~. In the context of englacial debris transport, this implies that the initial debris concentration is constant for an initial control volume of ice being tracked (i.e. seen from Lagrangian perspective). The incompressibility assumption demands also the absolute values of concentration to remain constant during transport when following the initial control volume of ice as it is becoming deformed during transport. To solve the transport problem mathematically, we take an ~~Eularian~~ Eulerian approach. The accuracy of the results is directly related to mesh size. If the mesh size was chosen infinitesimally small, the concentration features would recover, over the entire transport path, their initial values and sharp layers at their boundaries (if initial debris inputs are delineated by sharp boundaries). As a

consequence of a fixed mesh, the bigger the mesh size, the greater the amount of numerical smearing in the simulations which results in a decrease of maximum and marginal concentration values and a smearing towards the edges of the concentration features. This problem is inherent to the method chosen but can be dealt with by applying an appropriate mesh size, such that numerical smearing is minimized according to the application of interest. ~~In a later stage of model framework development, we will add~~

The model presented here forms part of an envisaged fully-integrated model framework that, by incorporating a (1) ~~a~~ free surface evolution scheme including debris-aware mass balance subroutines and (2) ~~a~~ transport model for debris at the glacier surface interacting with the mass balance subroutines~~. This fully integrated model framework~~ , will be capable of simulating the transient response of debris-covered glaciers, with predetermined debris inputs, to a changing climate.

This paper is structured as follows: ~~Section~~Sect. 2 provides details about the equations governing ice flow and how the transport problem is addressed from a mathematical perspective. ~~Section~~Sect. 3 describes the numerical schemes employed. ~~Section~~Sect. 4 details the test simulations performed, the results of which are presented in ~~See~~Sect. 5 and discussed in terms of model performance, limitations and applicability in ~~See~~Sect. 6. Conclusions and outlook are presented in ~~See~~Sect. 7.

2 Mathematical formulation

2.1 Full-Stokes formulation for ice flow

Ice is treated as an incompressible, non-linear viscous fluid, whose velocity and pressure distribution can be described by the incompressible stationary Stokes equations on a spatial domain $\Omega \in \mathbb{R}^3$, representing the ice body:

$$-\nabla \cdot [\eta(\nabla \mathbf{u} + (\nabla \mathbf{u})^{T\top})] + \nabla p = \rho_{\text{ice}} \mathbf{g} \quad \text{in } \Omega \tag{1a}$$

$$\nabla \cdot \mathbf{u} = 0 \quad \text{in } \Omega. \tag{1b}$$

Here $\mathbf{u}$ is the 3D velocity field, η is the non-linear viscosity, p is the pressure, ρ_{ice} is the density of ice and $\mathbf{g}$ is the acceleration due to gravity. The density of ice is assumed to be constant in time and space. By including the standard rheology of ice (Glen, 1955; Nye, 1957), its non-linear viscosity can be described by:

$$\eta = \frac{1}{2} A^{\frac{-1}{n}} \dot{\epsilon}^{\frac{(1-n)}{n}}, \tag{2}$$

where $\boldsymbol{\varepsilon} = 1/2(\nabla \mathbf{u} + (\nabla \mathbf{u})^{T\top}$ is the strain rate tensor and $\dot{\epsilon} = \sqrt{0.5 \varepsilon_{ij} \varepsilon_{ji}}$ is the effective strain rate. A represents the Glen rate factor and n the Glen flow law exponent. The computational domain Ω is confined by a free surface boundary at the ice-air interface ($\partial\Omega_{\text{top}}$) satisfying:

$$2\eta \boldsymbol{\varepsilon} \cdot \mathbf{n} - p\mathbf{n} = 0 \quad \text{on } \partial\Omega_{\text{top}}, \tag{3}$$

where $\mathbf{n}$ is the outward pointing surface normal. At the ice-bedrock interface ($\partial\Omega_{\text{bed}}$) either a no-slip (Dirichlet-) boundary condition (Eq. 4a) or, for glaciers where basal sliding contributes to total movement, an alternative ice-bedrock (Neumann-)

boundary condition can be applied (Eq. 4b) in conjunction with an appropriate sliding law conditioning the interface parallel ice velocity components at the glacier base.

$$\mathbf{u} = 0 \quad \text{on } \partial\Omega_{\text{bed}} \tag{4a}$$

$$\mathbf{u} \cdot \mathbf{n} = 0 \quad \text{on } \partial\Omega_{\text{bed}} \tag{4b}$$

2.2 Advection of material within a glacier

To describe transport and associated deformation of advected material within a glacier, we employ the linear transient advection-diffusion equation:

$$\frac{\partial c}{\partial t} = \nabla \cdot (D \nabla c) - \nabla \cdot (\mathbf{u} c) + r \quad \text{in } \Omega \tag{5a}$$

$$c = 0 \quad \text{on } \partial\Omega_D, \text{ on } \partial\Omega_0, \tag{5b}$$

where c is the concentration of the material, $D \geq 0$ is the diffusion coefficient, $\mathbf{u}$ is the divergence-free velocity field and r represents any internal sources or sinks. In the case of transport of debris through a glacier, it is reasonable to assume $r = 0$ and that material is predominantly transported by advection, therefore we currently neglect diffusion by setting D sufficiently small. As we focus on englacial transport in this study, we set $c = 0$ at the domain boundaries except the parts of the boundary where an input location is assigned ~~.~~ ($\partial\Omega_0$). Based on these assumptions and defining a constant diffusion coefficient D, Eq. 5 becomes:

$$\frac{\partial c}{\partial t} = D \nabla^2 c - \mathbf{u} \cdot \nabla c \quad \text{in } \Omega \tag{6a}$$

$$c = 0 \quad \text{on } \partial\Omega_0. \tag{6b}$$

At starting time t_0, a known initial concentration is given for all grid points on locations ($\mathbf{x}$) by:

$$c(\mathbf{x}, t = t_0) = c_0(\mathbf{x}) \quad \text{in } \Omega. \tag{7}$$

Apart from an initial concentration, material can enter the domain at the boundaries as a single input at time t_{input} or by a defined rate as a function of time and location.

3 Numerical schemes and model software

The model consists of three main components, (1) ice deformation (*icetools*), (2) adaptive mesh refinement according to concentration patterns (*refine_gl*) and (3) debris transport (*advect_gl*). All model components are individual open-source modules coded in python and utilizing the FEniCS framework (Alnæs et al., 2015; Logg et al., 2012a). Computations are performed on unstructured meshes (triangles in 2D (two-dimensions) and tetrahedrons in 3D), that allow for variable mesh size according to local requirements in spatial resolution and geometry complexity. Computational meshes are generated with *gmsh* (Geuzaine and Remacle, 2009), an open-source finite element mesh generator.

3.1 FEniCS software

FEniCS is an open-source project designed for automated solution of partial differential equations (PDEs) by finite element methods (FEM) (https://fenicsproject.org, Alnæs et al., 2015; Logg et al., 2012a). It includes several components such as DOLFIN (Logg and Wells, 2010; Logg et al., 2012c), FFC (Kirby and Logg, 2006; Logg et al., 2012b; Ølgaard and Wells, 2010) and FIAT (Kirby, 2004, 2012), which enable automatic solution of linear and non-linear problems once the variational forms of the PDEs are expressed in the Unified Form Language (UFL, Alnæs et al., 2014; Alnæs, 2012).

3.2 Ice deformation

3D ice velocities are computed using *icetools*, a parallelized, open-source full-Stokes model for ice flow (Jarosch, 2008) that solves Eq. 1~~, 2, 3 and 4~~. A mixed function space of continuous piecewise ~~linears and quadratics~~ quadratics and linears is used to compute ice velocity and pressure. The capability of the model to simulate 3D velocity fields for complex ice bodies has been demonstrated in previous studies (Jarosch, 2008; Jarosch and Gudmundsson, 2012). Initial versions of *icetools* accounted for stress-dependent ice viscosity using a Picard-iteration scheme, but here we employ an updated version, where the non-linear problem of including stress-dependent viscosity is solved by the Newton-Method.

3.3 Mesh refinement

Deline et al. (2015) collated statistics of the dimensions of deposits from massive rock slope failures onto glaciers documented since 1900. For the documented events, they found mean (maximum/minimum) deposit lengths (n=55) and final thickness (n=20) of $6.3\,(18.2/1.4)\,\mathrm{km}$ and $3.5\,(22.0/1.0)\,\mathrm{m}$ respectively. These values represent the upper limits on the likely dimensions of individual rockfall events onto glaciers, although megaslides could have larger dimensions. In order to resolve debris or ash deposits covering the range of these observations, computational meshes are required to have a spatial resolution in the sub–meter scale. In the case of simulating glaciers several kilometers long, this would lead to immense computational costs. Therefore, we take the approach of refining the mesh locally, i.e. only those areas where concentration is present. In order to avoid mesh refinement at every computation time step, we increase the area of refinement by a spatial radius $R_{\mathrm{cells}} = \mathbf{u}_{\mathrm{max}} dt_{\mathrm{ADV}} c_{\mathrm{ref}}$ surrounding the concentration features, where $\mathbf{u}_{\mathrm{max}}$ is the maximum velocity in the refined area, dt_{ADV} is the refinement time step (see Sect. 3.5) and c_{ref} is a positive defined constant. In this manner, the mesh is refined in an area that covers the actual concentration feature and the distance it can possibly be transported within the refinement time step.

For 2D simulations, mesh refinement is implemented entirely in python using the FEniCS software framework (Alnæs et al., 2015; Logg et al., 2012a). A function representing the coordinates (Fig. 2b) where the concentration exceeds a threshold (Fig. 2a) and R_{cells} is defined on the domain-wide coarse mesh (Fig. 2c). Using this function, the cells to be refined can be marked at any stage of mesh refinement. The marked cells are refined uniformly until all affected cells have an area smaller than a threshold c_{vol} (Fig. 2d). In this study, c_{vol} is set to $0.075\ \mathrm{m}^2$ (equivalent to an equilateral triangle of edge length 0.416 m), which, according to the findings in ~~See~~Sect. 5.1, is suitable to successfully represent englacial debris features originating from surface layer deposits of several meters in thickness. For 3D simulations, *gmsh* (Geuzaine and Remacle, 2009) is used to

create a new refined mesh at every refinement time step. Therefore, a domain-wide coarse mesh is updated with information on the coordinates where concentration exceeds a threshold. To create the new mesh, the cell size within the radius R_{cells} of these coordinates is set to L_{csize}. This parameter is representative of the average cell size within this area. In order to further reduce the number of required cells, the mesh is primarily refined in streamline direction. Therefore, the coordinate points are first shifted using the present velocity and a time step of $0.75\ dt_{\text{ADV}}$. As the refinement is based on the same domain-wide coarse mesh for each refinement time step, both approaches (2D and 3D mesh refinement) prevent over-refinement and at the same time, the need for mesh coarsening.

~~In adaptive~~ Adaptive mesh refinement strategies ~~,~~ often employ *a posteriori* error ~~estimators and indicators~~ estimation (e.g. John, 2000)~~are often~~ . The PDE is solved and the assigned error estimators and indicators are used to mark the cells for refinement and potentially coarsening. ~~An iteration of solving, computation of error estimators and indicators, marking and refinement of marked cells is performed~~ Subsequently, the marked cells become modified and the PDE is solved on the newly refined mesh. This process is repeated until the error ~~estimator falls~~ estimators and indicators fall below a user-defined tolerance ~~for all cells~~within every cell. This procedure can require many iterations, resulting in high computational costs. In the case of debris inclusions within glaciers, we deal with rather smooth concentration fields, except for sparse areas of high concentration that often, initially or over time, exhibit a band-like shape. Therefore, rather than focusing only on sharp layers that are the main contributors to high errors on too-coarse meshes, we perform the refinement on the entire area of high concentration. Instead of using ~~errors~~ error estimators and indicators to locate the cells for mesh refinement, our methods use a concentration-threshold, cell-based refinement indicator. This indicator is computed just once per refinement time step and all affected cells and those within a velocity-based distance (R_{cells}) are (a) refined until a problem-specific mesh size tolerance (c_{vol}) is achieved (2D) or (b) are created with a cells size prescribed by L_{csize} (3D) . ~~Comparing~~ The results of the benchmark test in ~~See~~Sect. 5.1 derived with our approach ~~and with~~ compare well with that derived using adaptive mesh refinement based on *a posteriori* error estimation (de Frutos et al., 2014), this demonstrates that our approach is an acceptable balance between accuracy and savings in computational costs. The 3D benchmark test in ~~See~~Sect. 5.1, demonstrates the suitability of the 3D mesh refinement approach.

3.4 ~~Time stepping~~

~~The refinement time step prescribes how often the refinement has to be performed and, in conjunction with the velocity field, defines the total number of cells in the mesh. For example, for a given englacial debris concentration, the total number of cells in the refined mesh increases with increasing refinement time step as the distance the debris inclusions are transported within this time step also increases. In order to minimize computational effort, the refinement time step has to be chosen according to the characteristics of the computer system that is used to run the computations. The computation time step for the advection module is derived using the Courant-Friedrich-Lewy condition, applied on the smallest cell size and the maximum velocity within the refined region. In this study, we apply Courant numbers ranging from $0.5 - 1.5$. The work of Bochev et al. (2004) combined with the tests in the supplementary material, show that the SUPG stabilisation scheme coupled~~

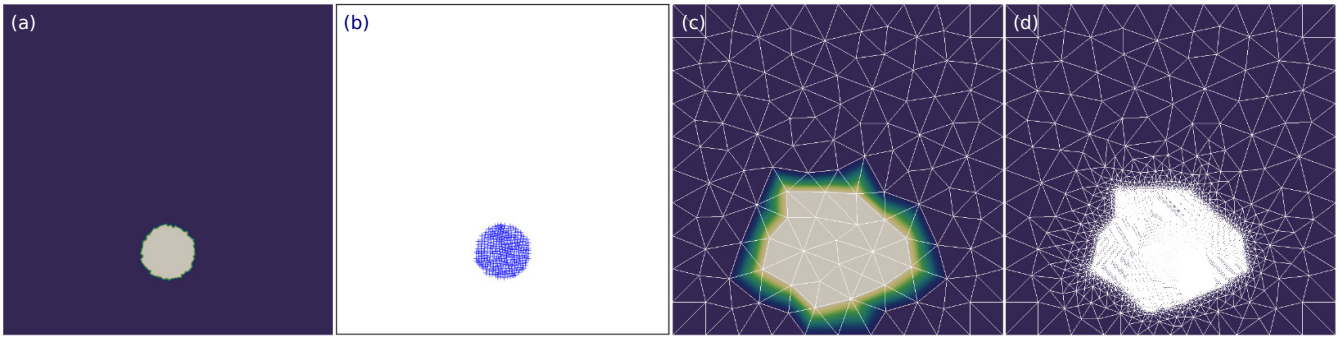

Figure 2. Illustration of mesh refinement. (a) ~~initial~~ Initial concentration field ~~with,~~ where bright colours indicate high concentration values. (b) ~~coordinate~~ Coordinate points of grid locations where concentration exceeds a threshold of 0.01. (c) ~~function~~ Function that shows high values, indicated by bright colours, at all cells of the coarse mesh that lie within the radius R_{cells} of the respective coordinate points in (b). (d) ~~representation~~ Representation of the final refined mesh.

~~to a Crank-Nicholson or an implicit Euler scheme for time-dependent advection-dominated, advection-diffusion problems is stable for this choice of Courant numbers.~~

3.4 Material transport

The transient advection-diffusion equation is discretized in time by an implicit Euler scheme and a standard continuous Galerkin FEM is used for the space discretization, separating the temporal and spatial discretizations. The concentration is expressed as a scalar function in a continuous piecewise linear function space. In the case of advection-dominated transport, solving Eq. ~~5~~ 6 via standard continuous Galerkin FEM leads to non-physical spurious oscillations (e.g. Bochev et al., 2004). In order to inhibit these spurious oscillations and ensure stability, we employ the Streamline-Upwind-Petrov-Galerkin (SUPG) approach (Hughes and Brooks, 1982). In this method, a residual-based stabilization term is added to the variational form and in this way introduces artificial diffusion to the system in streamline direction. The stabilization term is based on the the residual of Eq. ~~5~~ 6 including the time derivative and a mesh-size dependent stabilization parameter τ. Following John and Novo (2011) and Bochev et al. (2004), in the advection-dominated case (i.e. Peclet numbers greater than 3) we use a stabilisation term of $\mathcal{O}(h_K)$ and define it as $\tau = \frac{h_K}{2||\mathbf{u}||}$, where h_K is a measure of the local cell size and $\mathbf{u}$ is the divergence-free velocity field.

3.5 Time stepping

The refinement time step prescribes how often the refinement has to be performed and, in conjunction with the velocity field, defines the total number of cells in the mesh. For example, for a given englacial debris concentration, the total number of cells in the refined mesh increases with increasing refinement time step as the distance the debris inclusions are transported within this time step also increases. In order to minimize computational effort, the refinement time step has to be chosen according to the characteristics of the computer system that is used to run the computations.

The computation time step for the advection module is derived using the Courant-Friedrich-Lewy condition, applied on the smallest cell size and the maximum velocity within the refined region. In this study, we apply Courant numbers ranging from 0.5 – 1.5. The work of Bochev et al. (2004) combined with the tests in the supplementary material, show that the SUPG stabilisation scheme coupled to a Crank-Nicholson or an implicit Euler scheme for time-dependent advection-dominated, advection-diffusion problems is stable for this choice of Courant numbers.

4 Model simulations

Direct evaluation of our advection model against real world glacier cases is not possible at present because (i) comprehensive field measurements of englacial debris transport are not available and (ii) simulating the full glacier system would require further model development as outlined in ~~Sec~~Sect. 1.

Nevertheless, an evaluation of how well the model (a) performs and (b) reproduces structures observed in glaciers is important. To this end, we present results from specific numerical tests that benchmark the advection module, followed by ~~steady-state~~ glacier simulations for a 2D profile of an alpine valley glacier and an idealized 3D glacier geometry. In these glacier simulations the flow fields are computed by solving Eq. 1-4 for given geometries and are kept fixed as no mass balance routine is coupled to the model yet. The benchmark tests were performed to quantitatively ascertain that the numerics of our model adequately meet the requirements of the task in terms of mass conservation, numerical stability and prevention of non-physical spurious oscillations and numerical smearing. By comparing the results to those of the published tests, the suitability, stability and general performance of the advection module are evaluated. The glacier simulations are used to qualitatively evaluate how well the coupled iceflow - advection model reproduces glacial structures related to idealized debris inputs of various dimensions illustratively representing rockfall deposits, extensive ash layer or debris avalanche deposits and crevasse-fill in comparison to the structures predicted by theory or observed in the field.

4.1 Benchmark tests

The ~~Numerical~~ numerical Examples 1 and 2 in Bochev et al. (2004) are chosen to demonstrate the effect of the SUPG stabilisation approach in terms of reducing non-physical spurious oscillations that are a known problem for standard continuous Galerkin FEM schemes in the case of advection-dominated problems, and the stability of this stabilisation scheme for a wide range of Courant numbers that control the time stepping. Details of this set of numerical tests are presented in the supplementary material and here we present only the results of the most demanding numerical test that we subjected the model to, which is Example 4 in de Frutos et al. (2014). This test is known as the "rotating three body problem" (LeVeque, 1996; John and Novo, 2011; de Frutos et al., 2014) and is a standard test for computing advection of a scalar quantity in an incompressible flow field using the transient advection-diffusion equation in the advection-dominated case. Furthermore, in the study of de Frutos et al. (2014), the capabilities of *a posteriori* error-based adaptive mesh refinement are evaluated. By comparing the published results to those reproduced with our implementation of adaptive mesh refinement, we evaluate our method. In the "rotating three body problem", a slotted cylinder, a hump and a conical body undergo clockwise rotation in a divergence-free velocity field.

A visualisation of the velocity field is given in Fig. A4a in the supplementary material. In order to reproduce the results with our model, we set up the velocity field, initial and boundary conditions as described in Example 4 in de Frutos et al. (2014) for an advection-dominated case ($D = 10^{-6}$ m^2 s^{-1}). However, we employ the mesh refinement and time stepping described in ~~See~~Sect. 3 and redefine the model domain as $\Omega = (0,100) \times (0,100)$ meters. By doing this enlargement, the size of concentration features becomes comparable to the size of debris inputs in the glacier simulations. Initializing the mesh refinement with the same cell area threshold as is used in the glacier simulations, allows us to estimate the level of accuracy that we can achieve in the glacier cases. Here, we present ~~two different settings for mesh refinement~~ results of computations using two different refinement time steps, (a) small refinement time step of $0.01\,\pi$ s and (b) a larger refinement time step of $0.1\,\pi$ s. This results in (a) 200 and respectively for (b), in 20 refinement time steps for a full rotation of $2\,\pi$ ~~(T~~s (t_{total}). The computation time step is derived using a Courant number of 0.5. In order to evaluate the chosen cell area threshold, we perform convergence tests where (a) ~~$\|u_{\text{h}} - u_{\text{e}}\|_{\text{L}_2}$~~ $\|c_{\text{h}} - c_{\text{e}}\|_{\text{L}_2} = \sqrt{\sum_{k=1}^{n} (c_{\text{h}_k} - c_{\text{e}_k})^2}$ the L2 norm of the error between the computed finite element solution c_{h} and the exact solution c_{e}, where n is the number of computation locations, and (b) the Root Mean Square (RMS) error between the computed finite element solution and the exact solution for different cell size thresholds are computed. Therefore, we first compute the exact solution on the same mesh that is used in the finite element solution. To subject the model to an even more severe test, a second set of simulations is performed where the velocity field is prescribed as a swirling flow (LeVeque, 1996), but all other settings remain identical. Due to the swirling flow, the shapes of the three bodies become deformed but at total time (~~T~~t_{total}, at $t = 1.5$ s), the three bodies recover their initial shape. An animation of the swirling flow is included in the supplementary material.

To test the model capabilities in 3D, we reproduce the numerical test described in Christensen (1993), where a sphere of high concentration undergoes rotation. In this test, the velocity field is constructed in a manner, that the shape of the sphere is deformed throughout the rotation, but after a full rotation of 2π (~~T~~s (t_{total}), the sphere recovers its initial shape. A visualisation of the velocity field is given in Fig. A4b in the supplementary material. The model domain is defined as $\Omega = (0,32) \times (0,32) \times (0,40)$ meters and the mesh refinement is initialized with $L_{\text{csize}} = 0.15$ m. The refinement time step is set to $0.04\,\pi$ s and the Courant number to 0.5. By comparing the results to the analytical solution of the problem presented in Christensen (1993), model performance and chosen refinement settings can be evaluated.

4.2 Glacier tests

~~In all simulations presented here,~~ The purpose of these tests is to demonstrate the characteristics of debris transport within mountain glaciers, not to reproduce a particular event on a specific glacier. Hence, all velocity computations are initialized with a no-slip condition at the ~~glacier/bedrock~~ glacier-bedrock boundary, the flow law exponent n is set to 3 and the Glen rate factor A is set to 2.4×10^{-24} s^{-1}Pa^{-3}, a standard value for temperate ice (Cuffey and Paterson, 2010). The density of ice ρ_{ice} is set to 917 kg m^{-3}. The transport simulations are initialized with a debris concentration field c_0. X, Y, Z coordinates are used to identify a debris-deposition zone characterizing (a) a part of the ~~glacier/atmosphere, glacier/bedrock or glacier/sidewall~~ glacier-atmosphere, glacier-bedrock or glacier-sidewall interface that receives instant, continuous or variable debris input or (b) a localized debris inclusion as e.g. a remnant of a rockfall event or a ~~crevasse fill~~crevasse-fill. This is implemented by

assigning desired values of initial concentration at the respective locations to the function c_0, which is set to 0 everywhere else on the entire domain. In the presented glacier simulations, all debris inclusions have been deposited in a single event, hence they are all initialized as inclusions within the glacier, i.e. the entire glacier-atmosphere boundary belongs to Ω_0. In the 3D cases, the concentration is initialized with a smoothed function at the boundaries of the feature. This is done to represent it most efficiently in a continuous function space. Debris concentration that is transported beyond the boundaries of the glacier domain is removed from the system. The concentration itself is a scalar function able to have arbitrary numbers. It can be converted into actual debris mass as a function of the actual debris density and concentration of the initial debris deposit, i.e. the percentage of debris *versus* ice or snow in the initial volume of the deposit. In this study, we present model simulations for initial debris concentrations of the value 100, that can be scaled according to the case-relevant initial proportions of debris and ice. For example, in the case of an ash layer deposit, the initial ash concentration will likely make up to almost 100 %, compared to a mixed avalanche deposit that is likely to have much lower initial concentrations of debris *versus* snow or ice.

4.2.1 2D glacier test

For the 2D glacier test simulation, a 100 m spatial resolution longitudinal profile of bedrock and glacier surface for Haute Glacier d'Arolla was downloaded from the Ice Sheet Model Intercomparison Project (ISMIP) website (http://homepages.ulb.ac.be/~fpattyn/ismip/). These data represent the glacier in 1930, based on digitization of data from (Blatter et al., 1998), further described in (Pattyn, 2002). The longitudinal profile of 1930 is 5 km long. Haute Glacier d'Arolla is an alpine valley glacier with supraglacial debris covering approximately 10% of the glacier surface in 2012 (Reid et al., 2012).

In this test, we apply idealized debris inputs in the glacier accumulation area and track the evolution of the internal debris concentration while being transported in a ~~steady-state~~ fixed velocity field. For the 2D glacier profile, horizontal and vertical velocity components are shown in Fig. 3. In the supplementary material, Fig. A6 shows the surface velocity computed with a Glen rate factor $A = 10^{-16}$ a^{-1}Pa^{-3} as used in ISMIP, demonstrating that our model reproduces the ISMIP results in Pattyn et al. (2008). Five debris features of different size and input location are prescribed at varying time intervals (Fig. 4). ~~Thereby,~~ These debris deposits of varying size, shape and location of deposition were chosen to facilitate analysis of the interplay ~~of~~ between debris input location, deformation during transport and the ~~emergence location is possible~~zone of emergence. At $t = 0$, the prescribed initial debris concentration field consists of a circular debris inclusion centered at $x = 500$ m and $z = 3052$ m with a radius of 25 m (C0), a group of three ~~crevasse fills~~ crevasse-fills of $2-5$ m width and $50-75$ m length between $x = 1800$ m and $x = 1900$ m (CRV) , and a ca. 4 m thick debris layer covering the glacier surface between $x = 296$ m and $x = 854$ m of its length (D1). Subsequently, further debris layers are prescribed as follows: after 25 years, a ca. 9.5 m thick layer is deposited on the glacier surface between $x = 1000$ m and $x = 1600$ m (D2), and after 50 years another layer of ca. 5 m thickness is deposited between $x = 300$ m and $x = 1950$ m (D3). The circular inclusion and the debris layer deposits were prescribed to provide tight constraints on the shapes, whereas the vertical inclusions were initialized having irregular shaped boundaries considered more representative for actual ~~crevasse fills~~ crevasse-fills of variably sized debris material. The entire simulation, displayed in the video of the supplementary material, covers 90 years. The mesh refinement is initialized with $c_{\text{vol}} = 0.075$ m^2,

the refinement time step is set to 0.2 years and the Courant number to define the computation time step is set to 0.5.

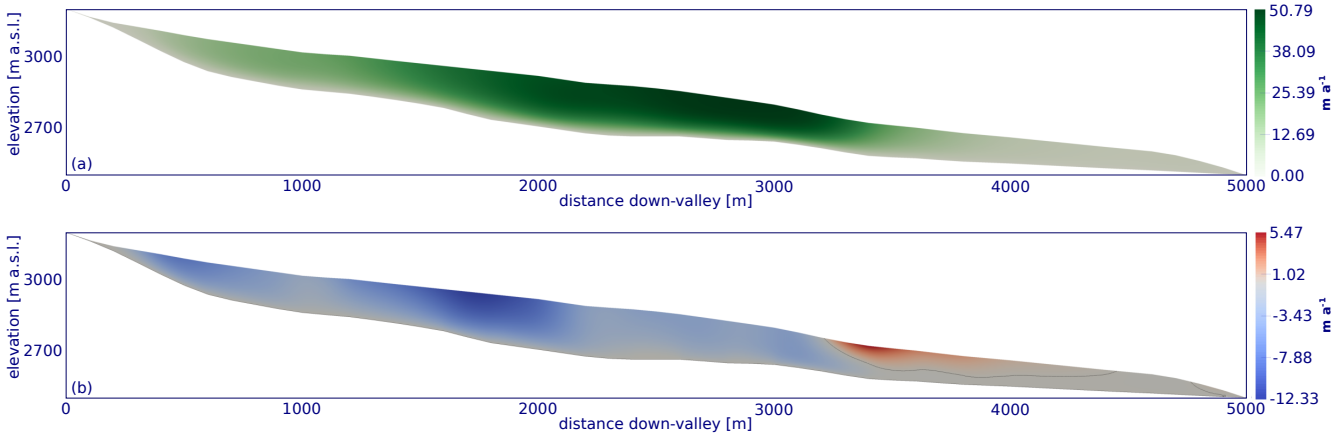

Figure 3. Velocity components computed with *icetools* for the 2D longprofile of Haute Glacier d'Arolla. ~~In~~ (a) ~~horizontal~~ Horizontal velocity (ma^{-1}) and (b) vertical velocity (ma^{-1}) and contour line of zero vertical velocity in grey.

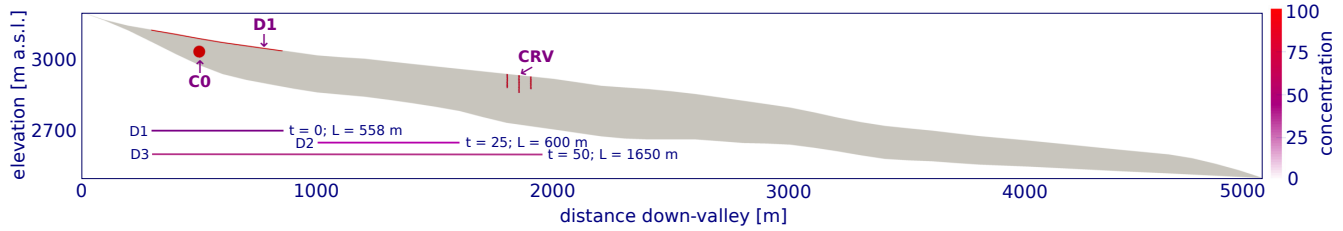

Figure 4. Debris concentration at time step t = 0 years, where C0 indicates the circular debris inclusion, D1-D3 the surface debris layer deposits and CRV the crevasse-fills. The horizontal lines indicate the location of ~~further~~ the debris ~~layers that are deposited at t = 25 and t = 50 years~~layer deposits including their time of deposition. L indicates the horizontal distance of the glacier surface where debris is deposited.

4.2.2 Idealized 3D glacier test

In the 3D glacier test, we perform simulations for an idealized glacier geometry. The geometry represents a valley glacier, including topographically-induced complexities such as a wide accumulation basin leading to a narrow valley, a bump in the bedrock geometry, as well as a turn of the valley itself. In this manner, topographic features that control ice flow in an alpine setting are represented, though idealized to reduce computational effort. The idealized ice geometry and the computed 3D velocity field is shown in Fig. 5. In this test, the mesh refinement is initialized with $L_{\mathrm{csize}} = 0.4$ m, the refinement time step is set to 0.4 years and the Courant number to 1.5.

The simulation is initialized with a spherical debris inclusion centered at $x = 0$ m, $y = 0$ m and $z = 270$ m in the accumulation area with a radius of 9.5 m. This initial concentration is chosen to aid visualization of the transport and deformation rather than to best represent likely en- and supraglacial debris deposits.

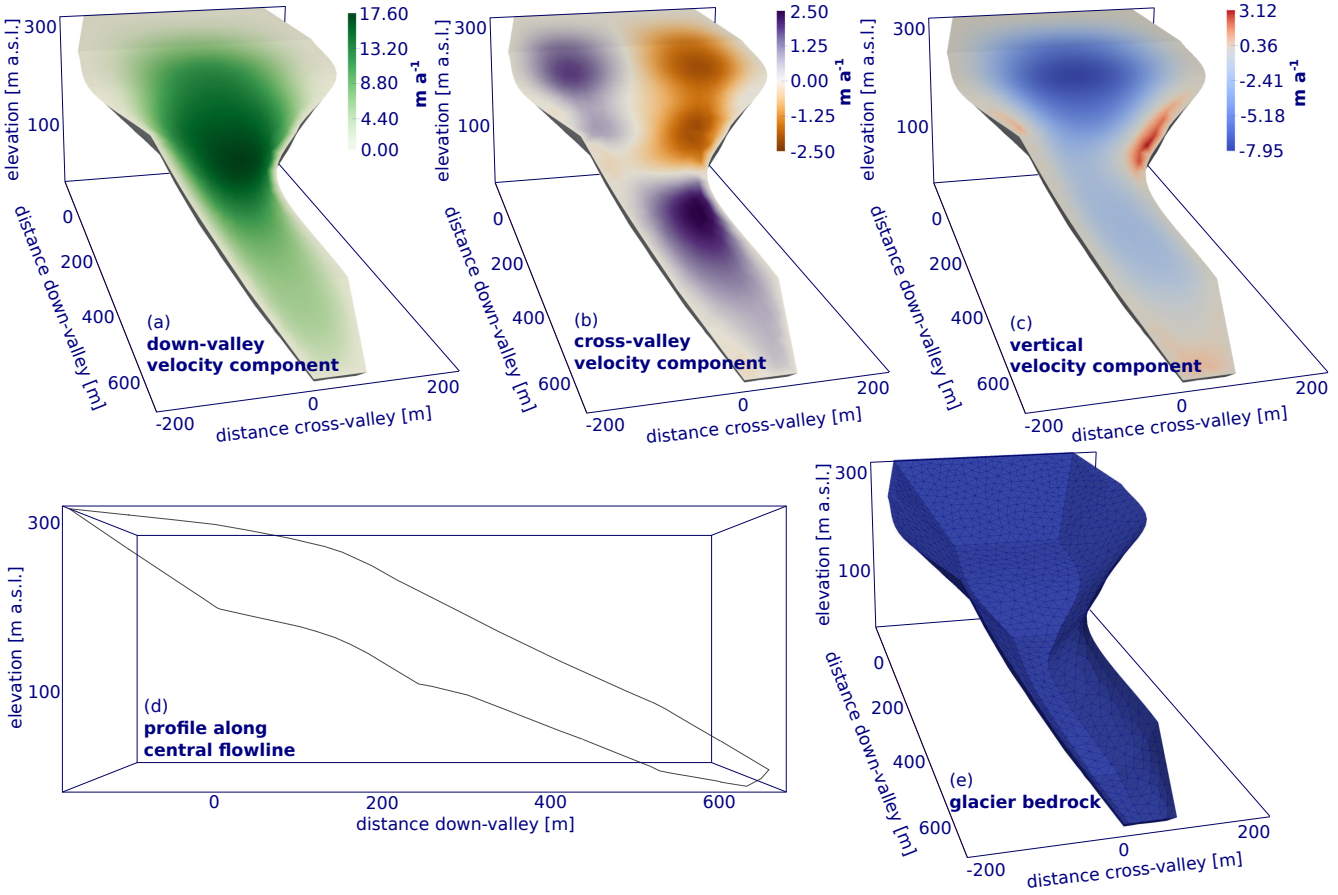

Figure 5. Idealized geometry and computed velocity components (ma^{-1}) for the 3D glacier case. (a) ~~downglacier~~ Down-valley direction (along x-axis), (b) ~~vertical~~ cross-valley direction (along ~~z-axis~~y-axis) and (c) ~~cross-glacier~~ vertical direction (along ~~y-axis~~z-axis), (d) approximate 2D down-valley profile along the central flowline and (e) glacier bedrock geometry.

5 Results

5.1 Benchmark tests

~~The results of~~ Our results of reproducing Examples 1 and 2 ~~reproduced following~~ in the numerical results in Bochev et al. (2004) are shown in Figs. A2 and A3 in the supplementary material. These simulations demonstrate the efficiency of our

SUPG algorithm implementation for reducing non-physical spurious oscillations in the solutions and allow us to choose suitable Courant numbers to ensure numerical stability.

The results of the "rotating three body problem" (de Frutos et al., 2014) are shown in Fig. 6, ~~exemplary~~ for the refinement time step $0.1\,\pi$ s. The results as well as animations for all sets of tests can be found in the supplementary material. In Fig. 6~~(~~a-c~~)~~, the initial condition, the solution after a full rotation of 2π s and the solution on the underlying mesh are shown. The shapes of the concentration features are well recovered in the case of both refinement time steps (see Fig. 6b for refinement time step $0.1\,\pi$ s and Fig. A5b in the supplementary material for refinement time step $0.01\,\pi$ s). Positive and negative oscillations in the solution are shown in Fig. 6~~(~~d-e~~)~~. The highest oscillations occur where the gradients in concentration are strongest, i.e. at the walls of the slotted cylinder. To measure the magnitude of remaining spurious oscillations in the solution, the difference of the maximum and minimum value of the solution is given in de Frutos et al. (2014). In our results, for case (a) $max(u) - min(u) = 1.2526$ with 87773 cells in the final mesh, whereas for case (b) $max(u) - min(u) = 1.2524$ with 142792 cells in the final mesh. These oscillations are slightly higher, but comparable to the values of $1.1010 - 1.1301$ reported in de Frutos et al. (2014). The total number of cells in the final meshes is larger in our computations, as the mesh refinement is performed in an interval of (a) $0.01\,\pi$ s or (b) $0.1\,\pi$ s and not individually for every computation time step. Mass loss is $< 0.009\%$ for both refinement time steps. Results of the convergence test for decreasing cell area thresholds, that are required to drive the mesh refinement, are shown in Fig. 6f. The chosen cell area threshold of 0.075 m^2 yields acceptable results. A further decrease leads to a drastic increase in computational costs, with only a small increase in model accuracy. ~~The results of the test simulations using the~~ Also, when the initial concentration pattern is subjected to a more complex, swirling flow (LeVeque, 1996)~~are presented~~, the results of these more challenging test simulations again show satisfactory model performance, as can be seen in Fig. 7 and Fig. A6 in the supplementary material.

The results of the 3D test following Christensen (1993) are illustrated in Fig. 8. An animation of the full rotation is given in the supplementary material. During the full rotation mass loss/gain is less than 0.01%. The shape of the concentration feature is in good agreement with the analytical solution as indicated by the ~~contour lines~~ isosurfaces of concentration (Fig. 8), just the highest concentrations (~~contour line~~ isosurface 90) are not captured well due to numerical smearing. This also causes the maximum value of concentration in the final solution to reduce to 83 (initially 100) and the spreading of very low concentrations (< 5) over a larger volume compared to the analytical solution.

5.2 2D glacier test

The upper boundary of the circular inclusion is initially located approximately 30 m beneath the glacier surface. During transport, it becomes severely elongated, as the upper part of the feature is transported faster with the ice flow than its lower part (Fig. 9a). After some travel time and sustained elongation, the vertical distance between the initially circular inclusion and the debris layer deposit D1 (Fig. 4) gradually decreases due to the vertical gradients in velocity (Fig. 9b). The initial surface emergence of the circular inclusion occurs later and further downglacier than any of the other imposed concentration features. It travels the longest distance and reaches the greatest depths within the glacier flow field.

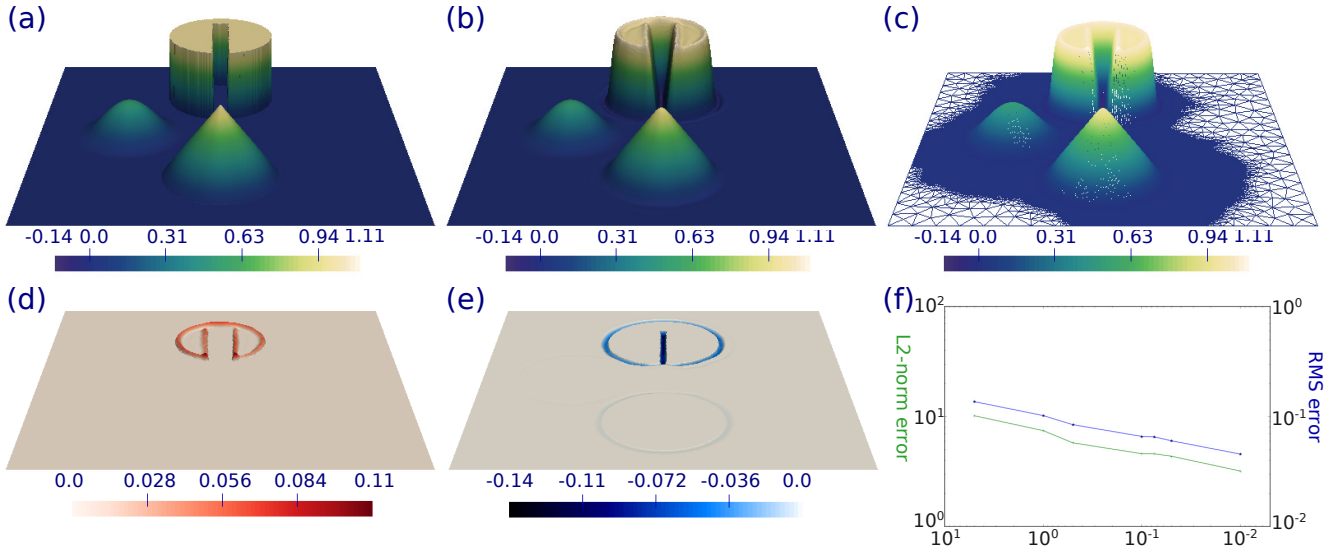

Figure 6. Results of 2D three body rotation test for refinement time step 0.1π s. ~~In~~ (a) ~~the initial~~ Initial condition, ~~in~~ (b) ~~the~~ solution after one full rotation and ~~in~~ (c) ~~the~~ solution after one full rotation on the underlying mesh~~is shown~~. ~~The data ranges from −0.14 to 1.11. In~~ (d) ~~overshoots~~ Overshoots (values greater than maximum initial value, as deviation from $max(c_{initial}) = 1.0$) and ~~in~~ (e) undershoots (values smaller than minimum initial value, as deviation from $min(c_{initial}) = 0.0$) at ~~T are presented. Colour scales show concentration values~~ t_{total}. ~~In~~ (f) ~~the results~~ Results of the convergence test ~~are shown with the L2 norm of the error on the left y-axis and the RMS-error on the right y-axis~~ as a function of mesh refinement parameter c_{vol}. Colour scales show concentration values.

The ~~crevasse fills~~ crevasse-fills are initially quasi-perpendicular to the glacier surface. As they are transported through the glacier, the vertical inclusions become deformed and exhibit a progressively more arcuate shape (Fig. 9d). These features reach the glacier surface and emerge first at $x = 2715$ m. They are removed from the glacier domain over the course of 31 years and over a distance of 580 m of the glacier surface. As they progressively emerge to the surface, the angle of outcrop rotates from vertical to upglacier dipping bands (Fig. 9d).

The layer-shaped debris inputs (D1-3 in Fig. 4) do not only have different characteristics such as length and thickness but are also deposited at different locations on the glacier surface. D1 first reaches the glacier surface at $x = 3450$ m and over a 90 year simulation period emerges over 109 m of the glacier surface. D2 first reaches the glacier surface at $x = 3190$ m and over a 90 year simulation period emerges over 281 m of the glacier surface. D3 first reaches the glacier surface at $x = 2645$ m and over a 90 year simulation period emerges over 645 m of the glacier surface. In comparison to D1 and D3, the upper limit of D2 is located ca. 700 m further downglacier. The zone of emergence is significantly shorter, it becomes less elongated and is exhumed in a shorter period of time, compared to D1 and D3. Another characteristic, observed in the modelling results, is a reduction in the distance between the debris bands further downglacier, coinciding with decreasing ice velocities in this part

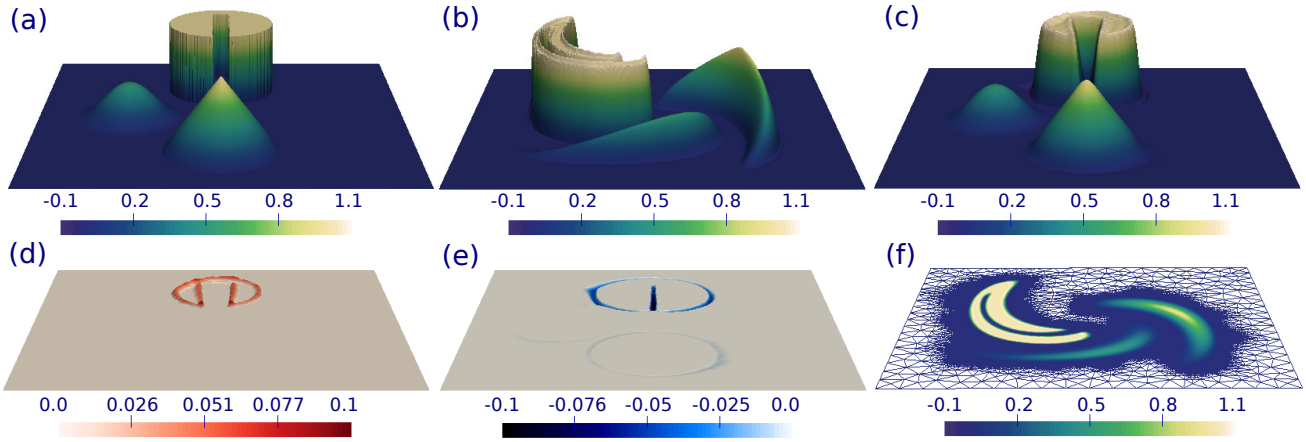

Figure 7. Results of 2D swirling flow three body test for refinement time step 0.01π s. ~~In~~ (a) ~~the initial~~ Initial condition, ~~in~~ (b) ~~the~~ solution at ~~$T/2$~~ $t_{\text{total}}/2$ and ~~in~~ (c) ~~the~~ solution at ~~T is shown. The data ranges from -0.1 to 1.1~~ t_{total}. ~~In~~ (d) ~~overshoots~~ Overshoots (values greater than maximum initial value, as deviation from $max(c_{initial}) = 1.0$), ~~in~~ (e) undershoots (values smaller than minimum initial value, as deviation from $min(c_{initial}) = 0.0$) at ~~T are presented~~ t_{total} and ~~in~~ (f) ~~the~~ solution at ~~$T/2$~~ $t_{\text{total}}/2$ on the underlying mesh~~is~~, shown in plan view. Colour scales show concentration values.

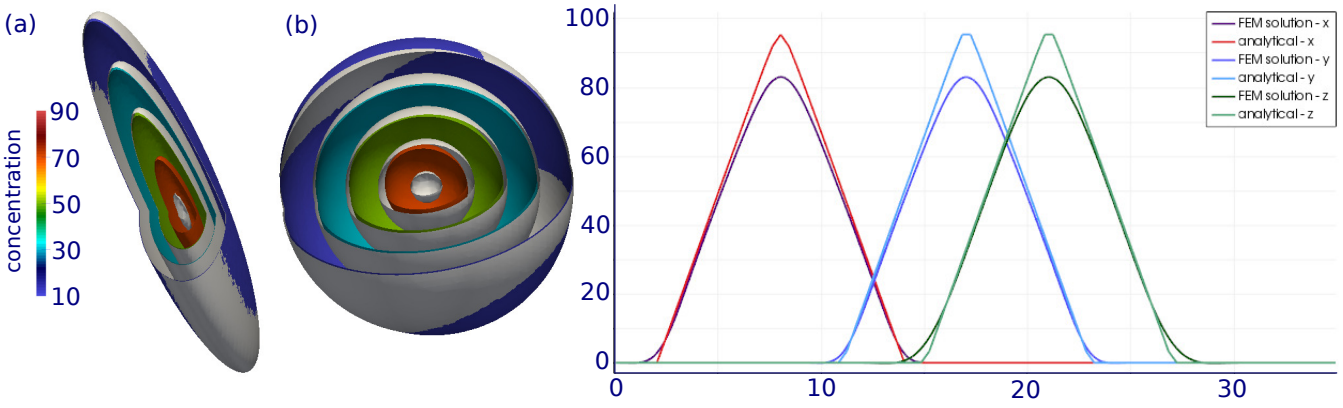

Figure 8. Results of 3D rotation test. ~~(a) shows contour lines~~ Isosurfaces of concentration 10, 30, 50, 70, and 90 for the FEM solution (in colour) and the analytical solution ~~at $T/2$ and~~ (in solid grey) at (~~b~~a) ~~the contour lines of concentration 10, 30, 50, 70, and 90 for the FEM~~ $t_{\text{total}}/2$ and ~~the analytical solution~~ at ~~T are shown~~(b) t_{total}. Note that for the FEM solution the ~~contour line~~ isosurface 90 is missing as the maximum values of concentration decreased to 87.5 (at ~~$T/2$~~$t_{\text{total}}/2$) and 83 (at ~~T~~t_{total}). ~~In~~ (c) ~~cross~~ Cross profiles parallel to the x-, y- and z-axis for the analytical and the FEM solution at ~~T are shown~~t_{total}.

of the glacier. The dip angle at the point of emergence to the surface differs between the three debris layer deposits and also changes as each layer feature is advected further downglacier.

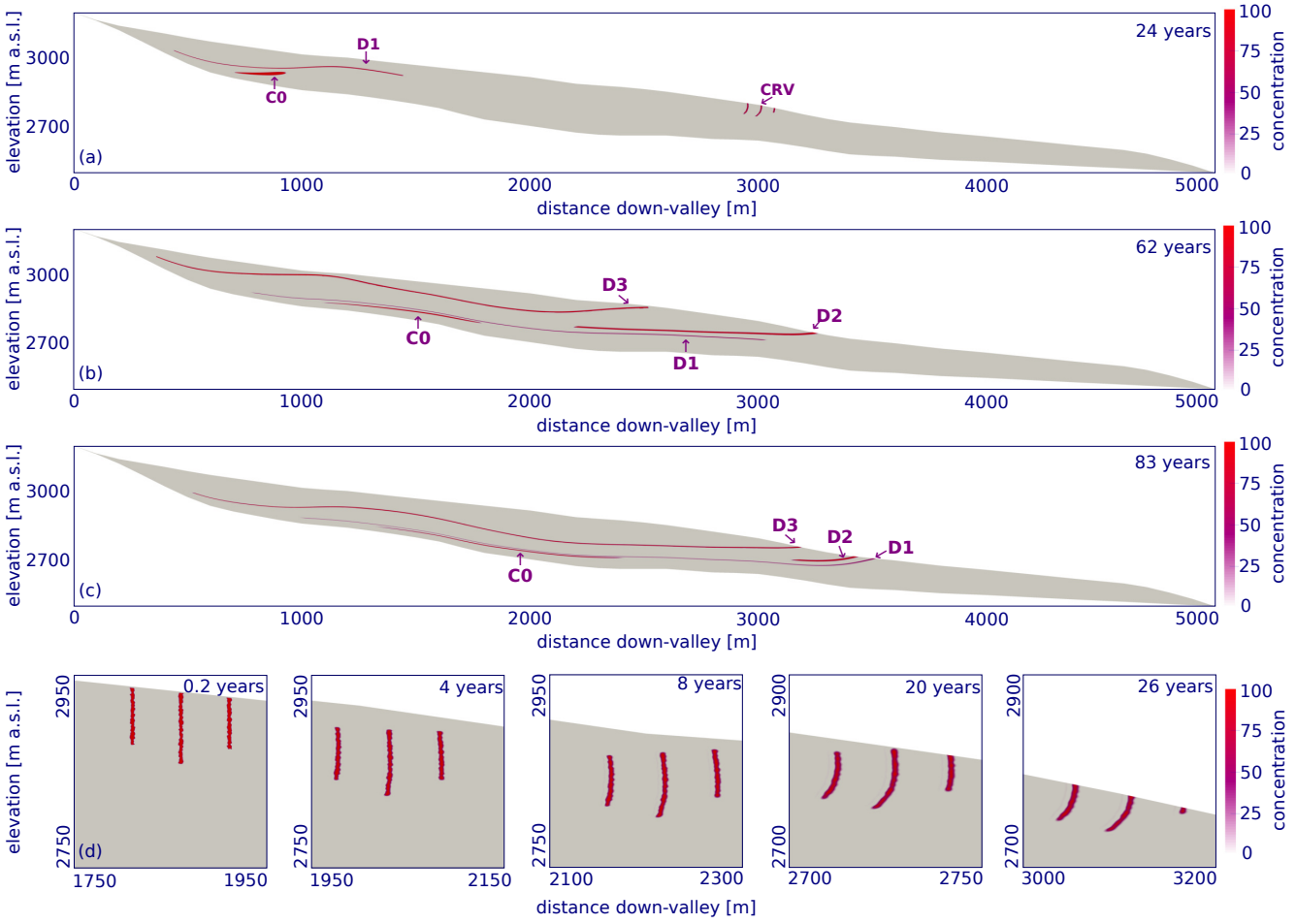

Figure 9. Results of the debris transport simulations for the 2D longprofile of Haute Glacier d'Arolla, where C0 indicates the circular debris inclusion, D1-D3 the surface debris layer deposits and CRV the crevasse-fills. ~~In~~ (a) ~~the debris~~ Debris concentration at 24 years, ~~in~~ (b) at 62 years and ~~in~~ (c) at 83 years after start of the simulations~~is shown~~. Concentrations are displayed in the range of 0 to 100, numerical oscillations as excursions beyond the initial values of 0 or 100 are of magnitude less than ± 17 and are truncated to the data limits. ~~In~~ (d) ~~a zoom~~ Zoom of the ~~crevasse fills~~ crevasse-fills at 0.2, 4, 8, 20 and 26 years after the start of the simulations~~is shown~~.

5.3 Idealized 3D glacier test

The deformation of englacial features shown in 2D is also represented in the 3D cases. The initially spherical inclusion becomes severely elongated in downglacier direction, forming a 'comet-like' tail as it is transported through the glacier. In addition to the downglacier elongation, where the glacier ~~is becoming~~ becomes narrower, the orographically left side of the debris inclusion is tilted upwards, and the centre of concentration is displaced laterally due to unequal lateral compression in the glacier flow

field as it rounds the bend in the idealized valley (Fig. 10). When layer-shaped features are introduced (not shown), they are deformed to form arcuate features that are concave in the vertical and downglacier direction.

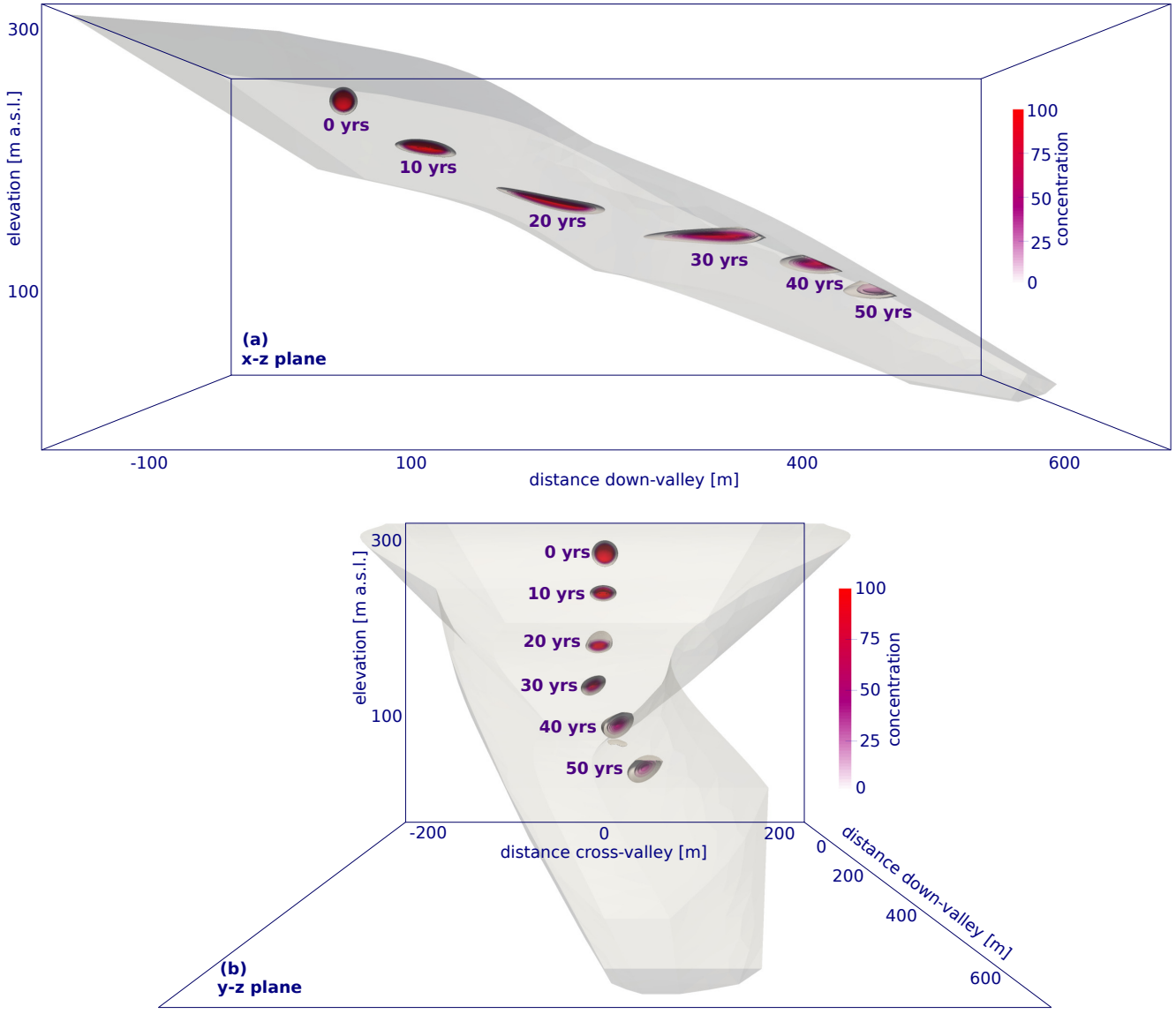

Figure 10. Results of the debris transport simulations for the 3D idealized glacier. Debris concentration ~~contour lines~~ isosurfaces of concentration 1, 10-100 in steps of 10 are displayed for a cut through (a) the x-z plane and (b) the y-z plane, as labelled in the figure. The ~~contour lines~~ isosurfaces shown refer to time 0-50 years after the start of the simulation in an interval of 10 years. Concentrations are displayed in the range of 0 to 100, numerical oscillations as excursions beyond the initial values of 0 or 100 are of magnitude less than ± 4 and are truncated to the data limits.

6 Discussion

6.1 Model capabilities and applicability

The debris transport and deformation modelled here reproduces structures analogous to those observed in structural glaciology, where elongated, sometimes cross-cutting debris layers outcrop with a range of dip angles at the glacier surface (Jennings et al., 2014; Goodsell et al., 2005). Not only can these structures be reproduced, but the 2D glacier simulations indicate that these elongated, band-shaped debris layers can form from initially fundamentally different debris deposits. ~~Both, (a) layer-shaped debris deposits on the glacier surface that are representative for~~ In these simulations, ash fall or avalanche events that uniformly cover wider portions of the accumulation area ~~and, (b) the circular inclusion~~ are included as layer-shaped debris deposits at the glacier surface. Rockfall events that result in a locally thick debris deposit are represented by a circular inclusion, as a possible remnant ~~of a localized rockfall event resulting in a thick debris deposit but limited in area,~~ thereof. Both distinctly different debris inputs become severely elongated and band-like shaped during transport. The degree of elongation depends on the input location and, hence, the trajectory through the glacier. In addition to horizontal stretching, the effect of lateral compressional flow is shown in the 3D glacier simulations.

The work of Kirkbride and Deline (2013) illustrates how both the thickness and angle of emergence of a debris band play a role in determining the initial thickness of an emergent debris deposit. This, in combination with the location of emergence is an essential prerequisite to predict the development and further evolution of debris cover. The simulations highlight that for spatially restricted debris deposition events, distinct debris bands form within the glacier that will lead to initially delimited areas of debris cover on the surface. Hence, an assumption of a uniform englacial debris distribution of constant englacial debris concentration (Naito et al., 2000) that would result in a continuously debris-covered glacier surface where surface ablation is occurring, might not reflect reality adequately. The model presented here allows us to simulate the advection of debris concentration through a glacier in great detail and therefore any resulting local concentration changes (Eulerian perspective), e.g. the deformation of debris deposit shape (Lagrangian perspective, cf. Fig. 10). Hence, for a given debris deposition event and glacier geometry, ~~to~~ we can quantify the timing and location of its emergence in the ablation zone, and how the location of maximum debris emergence from a debris band, and its dip angle will change over time. This is all critical information for determining how the spatial pattern of surface debris thickness will develop and evolve in time.

These results are also important in the context of the response of debris-covered glaciers to changes in climatic forcing or debris supply. Debris-covered glaciers are known to show distinctly different behaviour to clean-ice glaciers. This is due to the impact of debris cover on ice melt (Östrem, 1959; Mattson et al., 1993), which mainly depends on its thickness (Nicholson and Benn, 2006; Reid and Brock, 2010). In the case of negative mass balance-conditions, the emergence of thin debris cover at the upper end of the ablation zone can lead to locally enhanced melting, lower the surface slope and alter the dynamic regime of the glacier (Benn et al., 2012). When and where those transitions occur is also related to the location and rate of debris emergence.

The model presented here, which resolves the governing physical processes without ~~parameterisation~~parameterization, and is based on a comprehensive numerical framework, offers a powerful tool with which to examine the validity of assumptions

made in simpler models. For example, this model can be used to explore how the manner of prescribing debris (localized or distributed, spatially variable or constant, frequent or rare) affects the manner in, and timescales over, which a surface debris cover develops. This is valuable in the study of poorly understood earth systems like debris-covered glaciers, which evolve over timescales too long to allow real world observations to answer these questions. The model presented here can be used to track the passage of any material through the glacier - under the assumption that the transported material itself is not significantly altering the glacier flow field. It therefore has potential applications not only for understanding the development of ~~supra-glacial~~ supraglacial debris layers, but also for interpreting observed structures in glaciers related to specific tephra deposits or rockfall events, for example. This model also offers the possibility to test the findings of studies that use patterns of englacial debris distribution on Antarctic debris-covered glaciers to infer climate information at orbitally-paced time scales (Mackay and Marchant, 2017).

6.2 Model performance and limitations

The numerical accuracy of the presented model is dictated by the refinement and stability thresholds selected and will also vary dependent on the dimensions of the debris inputs. Nevertheless, we have demonstrated that the model performs satisfactorily in comparison to benchmark standards in the literature, and that this performance quality applies to the given model set up and thresholds used to simulate the glacier cases presented.

The ratio of debris input size *versus* the total size of the glacier requires very fine mesh sizes to actually resolve the debris inputs, their transport and associated deformation. For example, for the presented model set up in the 3D glacier example, the total number of cells is in the order of 10^8. This leads to high computational costs and the available computing resources impose constraints on the size of debris inputs the model is able to adequately simulate. In the case of localized debris inputs, our mesh refinement approach has the potential to reduce the total number of cells substantially compared to a mesh that is globally refined. In the simulations presented here, the parameters in the refinement module are chosen to produce a mesh that is as coarse as possible while guaranteeing mass conservation (> 99 %), numerical stability and limiting numerical oscillations and numerical smearing to the levels presented in the Results (~~See~~Sect. 5). Although numerical instabilities such as non-physical spurious oscillations and numerical diffusion are reduced efficiently by the approaches described in ~~See~~Sect. 3, numerical smearing cannot be eliminated completely. It's magnitude is controlled by the mesh resolution (see ~~See~~Sect. 1). Decreasing cell size reduces numerical diffusion, but limitations of computing power will in practice impose a lower bound on cell size. Therefore, the magnitude of numerical diffusion expected for a given model set-up should be taken into account when interpreting model results. The 2D benchmark tests show that the chosen cell area threshold of $0.075\ \mathrm{m}^2$ (for the 2D simulations) effectively limits non-physical spurious oscillations and numerical smearing below the levels presented in ~~See~~Sect. 5.1. In 3D, the constraints on cell size are even more restrictive in terms of numerical stability and numerical diffusion. However, increase in computational costs in 3D is non-linear. The results we show here in the case of an idealized 3D glacier geometry exhibit some numerical smearing, but are still suitable for glaciological applications. Higher accuracy for representing sharp concentration variations can easily be achieved by changing mesh refinement cell size variables at increased computational cost.

In practice, application details dictate the constraints on model accuracy required to be able to adequately resolve the problem at hand. In this respect, by performing multiple simulations, the model can also be used to quantify the smearing of concentration features that arises from the choice of a coarser, but computationally feasible, cell size. Thus the introduced error by coarse mesh size choices can be easily quantified.

7 Conclusions and outlook

We developed a model to simulate debris transport within glaciers based on an advection algorithm that is coupled to a full-Stokes ice flow model. To facilitate computations and provide the spatial resolution required to accurately represent observed debris inputs, a localized mesh refinement strategy is employed. In this manner, the deformation of debris inputs, arising from gradients in the glacier's velocity field, can be modelled explicitly. This is crucial, as the location of emergence as well as amount and rate of debris emergence on the glacier surface, depend on the deposition location of debris inputs and are subsequently controlled by englacial transport and deformation. This is the first model capable of resolving transport and deformation of debris inputs in this detail. The advection algorithm combined with the full-Stokes approach offers the potential to model englacial transport of various debris inputs and for complex glacier geometries. In a future step, coupling the englacial transport model presented here to a (i) debris-aware surface mass-balance scheme and (ii) supraglacial debris transport scheme will enable us to fully model the co-evolution of debris cover and glacier geometry, and the behaviour of debris-covered glacier systems in general. Additionally, this will offer a powerful means by which to evaluate simpler representations of debris cover development within glacier systems.

8 Code availability

A development version of the source code of the core components of the model and a test example of ~~See~~Sect. 4 is available under the GNU General Public License V3 and can be found at https://github.com/awirbel.

Acknowledgements. This work was funded by the Austrian Science Fund (FWF), projects: P28521 and V309. Thanks to Christoph Mayer for comments on an early draft of this paper.

References

Ackert, Jr., R. P.: A rock glacier/debris-covered glacier system at Galena Creek, Absaroka Mountains, Wyoming, Geogr. Ann. A, 80, 267–276, doi:10.1111/j.0435-3676.1998.00042.x, 1998.

Alnæs, M. S.: UFL: a finite element form language, in: Automated Solution of Differential Equations by the Finite Element Method, Volume 84 of Lecture Notes in Computational Science and Engineering, edited by Logg, A., Mardal, K.-A., and Wells, G. N., chap. 17, Springer, 2012.

Alnæs, M. S., Logg, A., Ølgaard, K. B., Rognes, M. E., and Wells, G. N.: Unified Form Language: A Domain-Specific Language for Weak Formulations of Partial Differential Equations, ACM T. Math. Software, 40, doi:10.1145/2566630, 2014.

Alnæs, M. S., Blechta, J., Hake, J., Johansson, A., Kehlet, B., Logg, A., Richardson, C., Ring, J., Rognes, M. E., and Wells, G. N.: The FEniCS Project Version 1.5, Archive of Numerical Software, 3, doi:10.11588/ans.2015.100.20553, 2015.

Anderson, L. S. and Anderson, R. S.: Modeling debris-covered glaciers: response to steady debris deposition, The Cryosphere, 10, 1105–1124, doi:10.5194/tc-10-1105-2016, 2016.

Benn, D., Bolch, T., Hands, K., Gulley, J., Luckman, A., Nicholson, L., Quincey, D., Thompson, S., Toumi, R., and Wiseman, S.: Response of debris-covered glaciers in the Mount Everest region to recent warming, and implications for outburst flood hazards, Earth-Sci. Rev., 114, 156–174, doi:10.1016/j.earscirev.2012.03.008, 2012.

Benn, D. I. and Evans, D. J. A.: Glaciers and Glaciation, Hodder Education, 2010.

Blatter, H., Clarke, G. K. C., and Colinge, J.: Stress and velocity fields in glaciers: Part II. Sliding and basal stress distribution, J. Glaciol., 44, 457–466, 1998.

Bochev, P. B., Gunzburger, M. D., and Shadid, J. N.: Stability of the SUPG finite element method for transient advection–diffusion problems, Comput. Method. Appl. M., 193, 2301–2323, doi:10.1016/j.cma.2004.01.026, 2004.

Bozhinskiy, A., Krass, M., and Popovnin, V.: Role of debris cover in the thermal physics of glaciers, J. Glaciol., 32, 255–266, 1986.

Christensen, J.: Testing Advection Schemes in a Three-Dimensional Air Pollution Model, Math. Comput. Model., 18, 75–88, 1993.

Clark, D. H., Steig, E. J., Potter, Jr., N., and Gillespie, A. R.: Genetic variability of rock glaciers, Geogr. Ann. A, 80, 175–182, doi:10.1111/j.0435-3676.1998.00035.x, 1998.

Cuffey, K. M. and Paterson, W. S. B.: The Physics of Glaciers, Academic Press, Burlington, MA, 4th edn., 2010.

de Frutos, J., García-Archilla, B., John, V., and Novo, J.: An adaptive SUPG method for evolutionary convection–diffusion equations, Comput. Method. Appl. M., 273, 219–237, doi:10.1016/j.cma.2014.01.022, 2014.

Deline, P., Hewitt, K., Reznichenko, N., and Shugar, D.: Rock Avalanches onto Glaciers, in: Landslide Hazards, Risks and Disasters, chap. 9, Elsevier, doi:10.1016/B978-0-12-396452-6.00009-4, 2015.

Geuzaine, C. and Remacle, J.-F.: Gmsh: a three-dimensional finite element mesh generator with built-in pre-and post-processing facilities, Int. J. Numer. Meth. Eng., 79, 1309–1331, 2009.

Glen, J. W.: The creep of polycrystalline ice, Proceedings of the Royal Society of London A: Mathematical, Physical and Engineering Sciences, 228, 519–538, doi:10.1098/rspa.1955.0066, 1955.

Goodsell, B., Hambrey, M. J., and Glasser, N. F.: Debris transport in a temperate valley glacier: Haut Glacier d'Arolla, Valais, Switzerland, J. Glaciol., 51, 139–146, 2005.

Hewitt, K.: Rock avalanches that travel onto glaciers and related developments, Karakoram Himalaya, Inner Asia, Geomorphology, 103, 66–79, doi:10.1016/j.geomorph.2007.10.017, 2009.

Hughes, T. J. R. and Brooks, A.: A theoretical framework for Petrov-Galerkin methods with discontinuous weighting functions: application to the streamline-upwind procedure., in: Finite Element in Fluids, edited by Gallagher, R. H., vol. 4, Wiley & Sons, 1982.

Jarosch, A. H.: Icetools: A full Stokes finite element model for glaciers, Computers & Geosciences, 34, 1005–1014, doi:10.1016/j.cageo.2007.06.012, 2008.

Jarosch, A. H. and Gudmundsson, M. T.: A numerical model for meltwater channel evolution in glaciers, The Cryosphere, 6, 493–503, doi:10.5194/tc-6-493-2012, 2012.

Jennings, S. J., Hambrey, M. J., and Glasser, N. F.: Ice flow-unit influence on glacier structure, debris entrainment and transport, Earth Surf. Proc. Land., 39, 1279–1292, doi:10.1002/esp.3521, 2014.

John, V.: A numerical study of a posteriori error estimators for convection–diffusion equations, Comput. Method. Appl. M., 190, 757–781, doi:10.1016/S0045-7825(99)00440-5, 2000.

John, V. and Novo, J.: Error analysis of the SUPG finite element discretization of evolutionary convection-diffusion-reaction equations, SIAM J. Numer. A., 49, 1149–1176, doi:10.1137/100789002, 2011.

Jouvet, G., Huss, M., Funk, M., and Blatter, H.: Modelling the retreat of Grosser Aletschgletscher, Switzerland, in a changing climate, J. Glaciol., 57, 1033–1045, 2011.

Kirby, R. C.: Algorithm 839: FIAT, A New Paradigm for Computing Finite Element Basis Functions, ACM T. Math. Software, 30, 502–516, 2004.

Kirby, R. C.: FIAT: numerical construction of finite element basis functions, in: Automated Solution of Differential Equations by the Finite Element Method, Volume 84 of Lecture Notes in Computational Science and Engineering, edited by Logg, A., Mardal, K.-A., and Wells, G. N., chap. 13, Springer, 2012.

Kirby, R. C. and Logg, A.: A Compiler for Variational Forms, ACM T. Math. Software, 32, doi:10.1145/1163641.1163644, 2006.

Kirkbride, M.: About the concepts of continuum and age, Boreas, 18, 87–88, doi:10.1111/j.1502-3885.1989.tb00376.x, 1989.

Kirkbride, M.: Ice-marginal geomorphology and Holocene expansion of debris-covered Tasman Glacier, New Zealand, Proceedings of an International Workshop Held at the University of Washington in Seattle, Washington, USA, 13–15 September 2000, IAHS Publication, 264, 211–217, 2000.

Kirkbride, M. P.: Debris-Covered Glaciers, in: Encyclopedia of Snow, Ice and Glaciers, edited by Singh, V. P., Singh, P., and Haritashya, U. K., pp. 180–182, Springer Netherlands, Dordrecht, 2011.

Kirkbride, M. P. and Deline, P.: The formation of supraglacial debris covers by primary dispersal from transverse englacial debris bands, Earth Surf. Proc. Land., 38, 1779–1792, doi:10.1002/esp.3416, 2013.

Konrad, S. K. and Humphrey, N. F.: Steady-state flow model of debris-covered glaciers (rock glaciers), Proceedings of an International Workshop Held at the University of Washington in Seattle, Washington, USA, 13–15 September 2000, IAHS Publication, 264, 255–266, 2000.

LeVeque, R.: High-resolution conservative algorithms for advection in incompressible flow, SIAM J. Numer. A., 33, 627–665, doi:10.1137/0733033, 1996.

Logg, A. and Wells, G. N.: DOLFIN: Automated Finite Element Computing, ACM T. Math. Software, 37, 1–28, doi:10.1145/1731022.1731030, 2010.

Logg, A., Mardal, K.-A., and Wells, G., eds.: Automated Solution of Differential Equations by the Finite Element Method, vol. 84 of *Lecture Notes in Computational Science and Engineering*, Springer, 2012a.

Logg, A., Ølgaard, K. B., Rognes, M. E., and Wells, G. N.: FFC: the FEniCS form compiler, in: Automated Solution of Differential Equations by the Finite Element Method, Volume 84 of Lecture Notes in Computational Science and Engineering, edited by Logg, A., Mardal, K.-A., and Wells, G. N., chap. 11, Springer, 2012b.

Logg, A., Wells, G. N., and Hake, J.: DOLFIN: a C++/Python finite element library, in: Automated Solution of Differential Equations by the Finite Element Method, Volume 84 of Lecture Notes in Computational Science and Engineering, edited by Logg, A., Mardal, K.-A., and Wells, G. N., chap. 10, Springer, 2012c.

Mackay, S. L. and Marchant, D. R.: Obliquity-paced climate change recorded in Antarctic debris-covered glaciers, Nat. Commun., 8, 14 194, doi:10.1038/ncomms14194, 2017.

Mackay, S. L., Marchant, D. R., Lamp, J. L., and Head, J. W.: Cold-based debris-covered glaciers: Evaluating their potential as climate archives through studies of ground-penetrating radar and surface morphology, J. Geophys. Res.-Earth, 119, doi:10.1002/2014JF003178, 2014.

Mattson, L. E., Gardner, G. S., and Young, G. J.: Ablation on Debris Covered Glaciers: an Example from the Rakhiot Glacier, Punjab, Himalaya, Proceedings of a Symposium Held at Kathmandu, Nepal 1992 – Snow and Glacier Hydrology, IAHS publication, 218, 289–296, 1993.

Menounos, B., Clague, J. J., Clarke, G. K., Marcott, S. A., Osborn, G., Clark, P. U., Tennant, C., and Novak, A. M.: Did rock avalanche deposits modulate the late Holocene advance of Tiedemann Glacier, southern Coast Mountains, British Columbia, Canada?, Earth Planet. Sc. Lett., 384, 154–164, doi:10.1016/j.epsl.2013.10.008, 2013.

Moore, P. L.: Deformation of debris-ice mixtures, Rev. Geophys., 52, 435–467, doi:10.1002/2014RG000453, 2014.

Naito, N., Nakawo, M., Kadota, T., and Raymond, C. F.: Numerical simulation of recent shrinkage of Khumbu glacier, Nepal Himalayas, Proceedings of an International Workshop Held at the University of Washington in Seattle, Washington, USA, 13–15 September 2000, IAHS Publication, 264, 245–254, 2000.

Nicholson, L. and Benn, D. I.: Calculating ice melt beneath a debris layer using meteorological data, J. Glaciol., 52, 463–470, 2006.

Nield, J. M., Chiverrell, R. C., Darby, S. E., Leyland, J., Vircavs, L. H., and Jacobs, B.: Complex spatial feedbacks of tephra redistribution, ice melt and surface roughness modulate ablation on tephra covered glaciers, Earth Surf. Proc. Land., 38, 95–102, doi:10.1002/esp.3352, 2013.

Nye, J. F.: The distribution of stress and velocity in glaciers and ice-sheets, Proceedings of the Royal Society of London A: Mathematical, Physical and Engineering Sciences, 239, 113–133, doi:10.1098/rspa.1957.0026, 1957.

Ølgaard, K. B. and Wells, G. N.: Optimisations for Quadrature Representations of Finite Element Tensors through Automated Code Generation, ACM T. Math. Software, 37, doi:10.1145/1644001.1644009, 2010.

Pattyn, F.: Transient glacier response with a higher-order numerical ice-flow model, J. Glaciol., 48, 467–477, 2002.

Pattyn, F., Perichon, L., Aschwanden, A., Breuer, B., de Smedt, B., Gagliardini, O., Gudmundsson, G. H., Hindmarsh, R. C. A., Hubbard, A., Johnson, J. V., Kleiner, T., Konovalov, Y., Martin, C., Payne, A. J., Pollard, D., Price, S., Rückamp, M., Saito, F., Souček, O., Sugiyama, S., and Zwinger, T.: Benchmark experiments for higher-order and full-Stokes ice sheet models (ISMIP–HOM), The Cryosphere, 2, 95–108, doi:10.5194/tc-2-95-2008, 2008.

Reid, T. D. and Brock, B. W.: An energy-balance model for debris-covered glaciers including heat conduction through the debris layer, J. Glaciol., 56, 903–916, 2010.

Reid, T. D., Carenzo, M., Pellicciotti, F., and Brock, B. W.: Including debris cover effects in a distributed model of glacier ablation, J. Geophys. Res-Atmos., 117, doi:10.1029/2012JD017795, 2012.

Reznichenko, N. V., Davies, T. R., and Alexander, D. J.: Effects of rock avalanches on glacier behaviour and moraine formation, Geomorphology, 132, 327–338, doi:10.1016/j.geomorph.2011.05.019, 2011.

Rowan, A. V., Egholm, D. L., Quincey, D. J., and Glasser, N. F.: Modelling the feedbacks between mass balance, ice flow and debris transport to predict the response to climate change of debris-covered glaciers in the Himalaya, Earth Planet. Sc. Lett., 430, 427–438, doi:10.1016/j.epsl.2015.09.004, 2015.

Shugar, D. H., Rabus, B. T., Clague, J. J., and Capps, D. M.: The response of Black Rapids Glacier, Alaska, to the Denali earthquake rock avalanches, J. Geophys. Res.-Earth, 117, doi:10.1029/2011JF002011, 2012.

Vacco, D. A., Alley, R. B., and Pollard, D.: Glacial advance and stagnation caused by rock avalanches, Earth Planet. Sc. Lett., 294, 123–130, doi:10.1016/j.epsl.2010.03.019, 2010.

Östrem, G.: Ice melting under a thin layer of moraine, and the existence of ice cores in the moraine ridges, Geogr. Ann., 41, 228–230, 1959.